

بِسْمِ اللَّهِ الرَّحْمَنِ الرَّحِيمِ
Palestine Polytechnic University



College of Engineering and Technology
Electrical and Computer Engineering Department
Industrial Automation Engineering

Design and Build of Single-Phase AC PM Synchronous Motor

Project Team

ANAS JUBER

MUATH ABDEEN

MOATAZ ISIEED

Project Supervisor

Dr. ABDEL-KARIM DAUD

Hebron-Palestine
June, 2008

Palestine Polytechnic University
College of Engineering and Technology
Electrical and Computer Engineering Department
Hebron-Palestine

Design and Build of Single-Phase AC PM Synchronous Motor

Project Team

ANAS JASSER JUBER

MUATH TAWFEEQ ABDEEN

MOATAZ NOAMAN ISIEED

In accordance with the recommendations of the project's supervisor, and the acceptance of all examining committee members, this project has been submitted to the department of electrical and computer engineering in the college of engineering and technology in partial fulfillment of the requirements of the Bachelor's degree in Industrial Automation Engineering.

Project supervisor signature

.....

Committee signature

.....

.....

.....

Department Head signature

.....

Dedication

We dedicate this simple work:

To our parents

To our brothers

To our friends

To our nation

To any person works hardly...

Acknowledgments

First and for most we should offer our thanks, obedience and gratitude to Allah.

Our appreciation to:

Palestine Polytechnic University

College of Engineering & Technology

Electrical & Computer Engineering Department

Our supervisor Dr. ABDEL-KARIM DAUD

Any one who helped us

Abstract

In this project the method of designing a Single Phase Permanent Magnet (SPPM) Synchronous motor is presented.

This motor has special design of stator and rotor. It is commonly used in low-power application.

The behavior of the motor as (starting, torque...) is described, and the starting behavior that depends on the initial position of the rotor is also described.

The network method (equivalent circuit) is used to analyze the magnetic circuit, and to perform the analytical solution of this project.

The achievement reaches is to build a Single Phase AC Synchronous PM Motor with specific dimensions.

A frequency converter is used as the control device to obtain suitable type of control for this motor.

There are growing applications for this motor, especially, in low-power like: automobile industry, central heating, and house appliances (washing machines, dishwasher).

Table of Contents

Signatures page	ii
Dedication	iii
Acknowledgment	iv
Abstract	v
Table of contents	vi
List of tables	vii
List of figures	ix
Chapter one	
INTRODUCTION	1
1.1 General Outlook	2
1.2 Project Objectives	6
1.3 Advantages of PM Synchronous Motor	6
1.4 Disadvantages of PM Synchronous Motor	6
1.5 Applications of the PM Synchronous Motor	7
1.6 Previous Studies	11
1.7 History of PM	12
1.8 Table of Cost	12
1.9 Time Plan	13
Chapter two	
AC MOTOR CLASSIFICATION	14
2.1 Single-Phase PM AC Motor	15
2.1.1. Single-Phase Synchronous Motors	15
2.1.2. Single-Phase Induction Motors	16
2.2 Reluctance Motor	17
Chapter three	
MOTOR DESIGN	19
3.1 Introduction	20
3.2 Rotor Parameter	22
3.2.1 Differential Rotor MMF And Permeance	23
3.2.2 Differential Air-Gap Permeance	25
3.2.3 Calculation of Reluctance Torque	28
3.2.4 Calculation of Peak Rotor Flux	29

3.3	Rest Position of the Rotor (θ_0)	33
3.4	Calculation of Stator Inductance	35
3.4.1	Simplification of Stator Magnetic Circuit	36
3.4.2	Fringing flux Calculation	38
3.4.3	Stator-Inductance Expression	40
Chapter four		
	MOTOR CONSTRUCTION	42
4.1	Stator	43
4.2	Rotor	47
Chapter five		
	SPEED CONTROL	51
5.1	Speed Control of PM Motor	52
5.2	PI Controller	53
5.3	Frequency Converter	54
5.3.1	Frequency Converter Principles	54
5.3.2	Variable Frequency	55
	Conclusion	58
	References	59
APPENDICES		60
A	Permanent Magnet Material	61
B	Motor Parameters Calculation	66

List of Tables

Table 1.1: Cost of the project	12
Table 1. : Time plan the of project	13
Table A.1: Magnetic characteristics of sintered NdFeB PMs manufactured in China	44
Table A.2: Physical properties of sintered NdFeB PMs manufactured in China.	45
Table A.3: Magnetic characteristics of bonded NdFeB PMs manufactured in China	45
Table A.4: Physical properties of bonded NdFeB PMs manufactured in China..	46
Table B.1: Motor parameters.....	48

List of Figures

Figure 1.1	Single-phase PM synchronous motor with asymmetrical stator magnetic circuit: (a) smooth nonuniform air gap, (b) stepped nonuniform air gap	2
Figure 1.2	Single-phase PM synchronous motor with symmetrical stator magnetic circuit: (a) smooth nonuniform air gap, (b) stepped nonuniform air gap	4
Figure 1.3	Speed and current versus time in self-starting mode for a two-pole synchronous motor with oscillatory starting: 1 - speed, 2 - current	4
Figure 1.4	An industrial robot (M - electric motor)	10
Figure 1.5	PM motors installed in a car	11
Figure 3.1	Electrical equivalent circuit of an SPPM motor	20
Figure 3.2	Magnetic equivalent circuit of the rotor of an SPPM motor	22
Figure 3.3	Typical B-H characteristics of a permanent magnet	23
Figure 3.4	Differential analysis of rotor parameters	24
Figure 3.5	Magnetic field solution results for several rotor positions	24
Figure 3.6	Analysis of air gap permeance density distribution	25
Figure 3.7	Normalized air gap permeance variation	27
Figure 3.8	Calculated reluctance torque against position	28
Figure 3.9	Representation of the fringing field at the rest position	30
Figure 3.10	Equivalent rotor shape with uniform air-gaps	31
Figure 3.11	Equivalent rotor shape with uniform air gaps for the rest position calculation	33
Figure 3.12	Field distribution just for stator excitation	35
Figure 3.13	Magnetic equivalent circuit for stator excitation	36

Figure 3.14	Magnetic circuit of the stator with a stepped-air gap	37
Figure 3.15	Stator magnetic circuit with simplified rotor gap	37
Figure 3.16	Simplified magnetic circuit of the stator	37
Figure 3.17	(a) Top view of the stator core with fringing regions (b) Approximate model of stator core for fringing calculations ...	39
Figure 4.1	Construction of stator	43
Figure 4.2	Stator (1) belt (2) stator body	44
Figure 4.3	Stator windings (drawing)	45
Figure 4.4	Stator windings (practical)	45
Figure 4.5	Stator design (3dmax)	46
Figure 4.6	(a) starting point of windings (b) ending point of windings	46
Figure 4.7	(a) starting point of windings (b) ending point of windings	47
Figure 4.8	Rotor design(1) Rotor (2) Two pairs of PM (drawing)	48
Figure 4.9	Rotor design (3dmax)	48
Figure 4.10	Final construction of motor (drawing)	49
Figure 4.11	Final construction of motor (3dmax)	49
Figure 4.12	Catia drawing of the project (3-D view)	50
Figure 5.1	Closed loop system of SPPM motor	52
Figure 5.2	PI controller	53
Figure 5.3	PI controller curve	53
Figure 5.4	Frequency converter block diagram	54
Figure 5.5	Relation between the voltage and frequency	55
Figure 5.6	Three phase frequency converter construction using Simplerer....	56
Figure 5.7	Single phase frequency converter construction using Simplerer...	56
Figure 5.8	Output voltage from rectifier	57
Figure 5.9	Output voltage from frequency converter	57

CHAPTER ONE

INTRODUCTION

1.1 General Outlook

1.2 Project Objectives

1.3 Advantage of PM Synchronous Motor

1.4 Disadvantage of PM Synchronous Motor

1.5 Applications of Permanent Magnet Motors

1.6 Previous Study

1.7 History of PM

1.8 Table of Cost

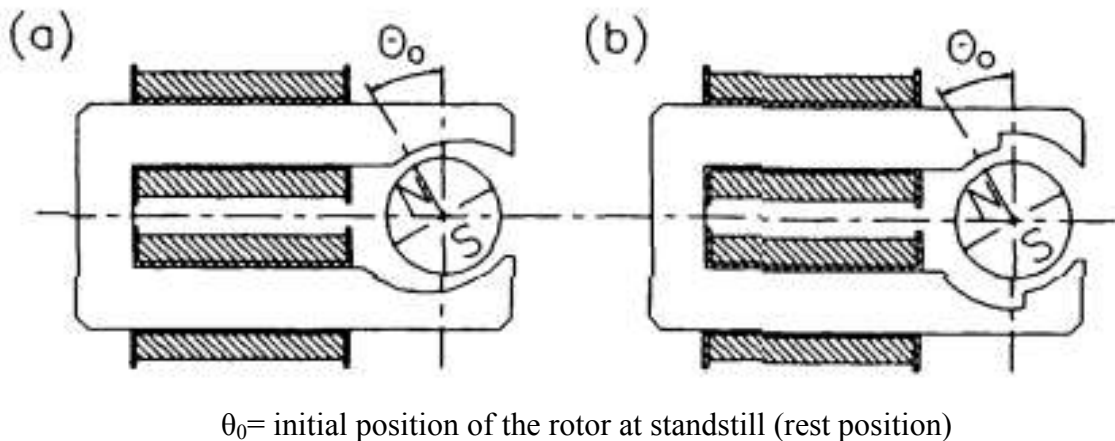
1.9 Time Plan

CHAPTER ONE

INTRODUCTION

1.1 General Outlook:

Single-phase permanent-magnet (SPPM) synchronous motors of the type shown in Fig. 1.1 have found growing applications especially in low-power household appliances. This is because this motor is well suited to mass production purposes and has a simple construction, and therefore has a cost advantage. Also, they are known to be more efficient than rival motors.



θ_0 = initial position of the rotor at standstill (rest position)
Fig. 1.1: Single-phase PM synchronous motor with asymmetrical stator magnetic circuit: (a) smooth nonuniform air gap, (b) stepped nonuniform air gap

A salient pole PM synchronous motor can be designed with nonuniform air gap as a self-starting motor. With regard to the stator magnetic circuit, two types of construction can be identified: U-shaped, two-pole asymmetrical stator magnetic circuit (Fig.1.1) and two-pole symmetrical stator magnetic circuit (Fig.1.2). In both asymmetrical and symmetrical motors, the nonuniform air gap can be smooth (Figs 1.1a and 1.2a.) or stepped (Figs 1.1b and 1.2b). The leakage flux of a U-

shaped stator is higher than that of a symmetrical stator. Nonuniform air gap, i.e., wider at one edge of the pole shoe than at the opposite edge, provides the starting torque as a result of misalignments of the stator and rotor field axes at zero current state.

The rest angle θ_0 of the rotor is the angle between the center axis of the stator poles and the axis of the PM rotor flux. These motors are only self-starting when, with the armature current $I_a = 0$, the angle $\theta_0 > 0$.

The largest starting torque is achieved when the rest angle $\theta_0 = 90^\circ$. The motor constructions shown in Fig. 1.1 limit the rest angle to $\theta_0 \leq 5^\circ \dots 12^\circ$, which consequently results in a small starting torque. The motors shown in Fig. 1.2 can theoretically achieve θ_0 close to 90° .

With zero current in the stator winding, the rest angle $\theta_0 > 0$ as the attractive forces between PM poles and the stator stack align the rotor center axis with the minimum air gap (minimum reluctance). After switching on the stator voltage the stator magnetic flux will push the PM rotor towards the center axis of the stator poles. The rotor oscillates with its eigenfrequency. If this eigenfrequency is close enough to the stator winding supply frequency, the amplitude of mechanical oscillations will increase and the motor will begin to rotate continuously. The eigenfrequency depends on the moment of inertia of the rotor and mechanical parameters. Larger motors with lower eigenfrequency thus require lower supply frequencies. It is important to know the dynamic behavior of these motors at the design stage to ensure the desired speed characteristics.

The advantages of these motors are their simple mechanical construction and relatively high efficiency at small dimensions and rated power. Owing to a simple manufacturing process, it is easier to fabricate the asymmetrical stator than the symmetrical stator. The symmetrical design can achieve almost the maximum possible starting torque (θ_0 close to 90°), while the asymmetrical

design has a relatively small starting torque. It should be noted that the direction of rotation in both designs cannot be predetermined.

The disadvantage is the limited size of the motor if it is to be utilized in its self-starting mode. Fig. 1.3 shows the oscillations of speed and current during start-up of a lightly loaded small motor. If the load increases, the oscillations of speed decrease more quickly than those in Fig. 1.3.

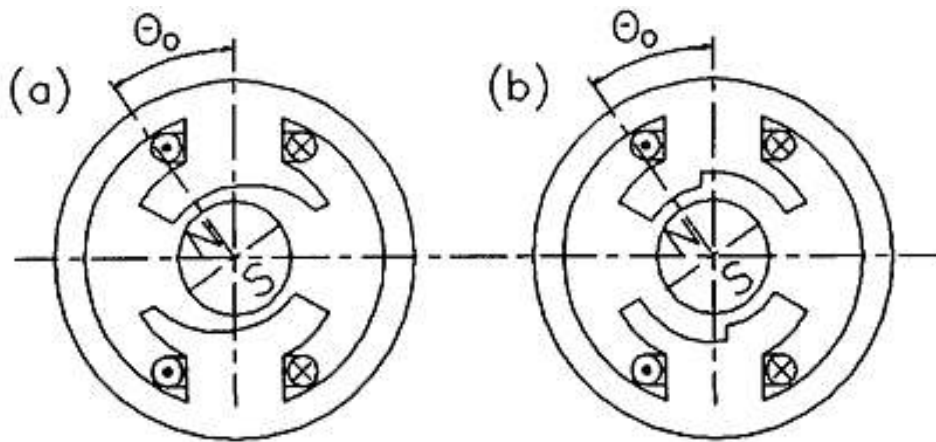


Fig. 1.2: Single-phase PM synchronous motor with symmetrical stator magnetic circuit: (a) smooth nonuniform air gap, (b) stepped nonuniform air gap.

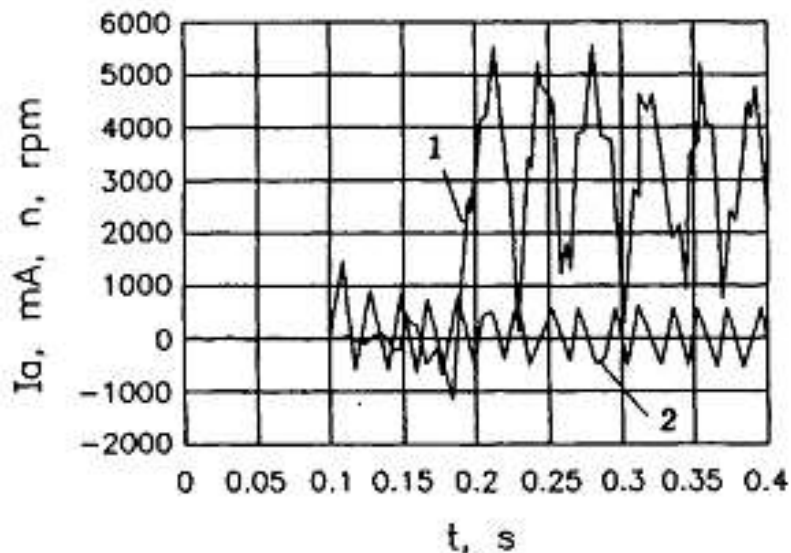


Fig. 1.3: Speed and current versus time in self-starting mode for a two-pole synchronous motor with oscillatory starting: 1 - speed, 2 - current

Simulation tools have the capabilities of performing dynamic simulations of motor drives in a visual environment so as to facilitate the development of new systems.

The use of PMs Motor in construction of electrical machines brings the following benefits:

- No electrical energy is absorbed by the field excitation system and thus there is no excitation loss which means substantial increase in the efficiency.
- Higher torque and / or output power per volume than when using electromagnetic excitation.
- Better dynamic performance than motors with electromagnetic excitation (higher magnetic flux density in the air gap)
- Simplification of the construction and maintenance
- Reduction of prices for some types of machines.

Of course, the use of very poor quality hard materials (steel or tungsten steel) soon discouraged their use in favor of electromagnetic excitation system; however, its application was limited to small and fractional horsepower DC commutator machines. Now they use ferrite magnets, and the ferrite PMs mounted on the stator will still be used in foreseeable future in road vehicles, toys, and household equipments [1].

PM synchronous motors are widely used in low and mid power applications such as computer peripheral equipments, robotics, adjustable speed drives and electric vehicles.

1.2 Project Objectives:

The aim of this project is to design and analyze a single-phase PM motor (SPPM) for educational purposes. The main goal of this project is to create a simple functional SPPM motor, rather than a highly complex and costly one.

The efficiency of this design will be carefully examined while using various materials for the rotor (reaction plate), and single-phase winding in the stator.

Many important parameters will be taken into account enable a relationship between the forces produced by these parameters. The experimental measured force is then compared to the calculated theoretical force. Any discrepancies between the values will be justified for.

1.3 Advantages of PM Synchronous Motor:

The advantages of PM synchronous motor is the higher accuracy to determine the desired position, higher efficiency with low power consumption, simple construction, and fast response with stability of performance, a PM motor can produce magnetic field in an air gap with no excitation winding.

1.4 Disadvantages of PM Synchronous Motor:

It can be overcome with a simple electronic aid and the motor may remain attractive for higher power levels. To be able to reach a sound decision on this issue, one needs to understand the factors (parameters) which control the performance of the motor. Based on this understanding, a design which satisfies the requirements may be reached.

1.5 Applications of Permanent Magnet Motors:

PM motors are used in a broad power range from mWs to hundreds Ws. There are also attempts to apply PMs to large motors rated at minimum Thus, PM motors cover a wide variety of application fields, from stepping motors for wrist watches, through industrial drives for machine tools to large PM synchronous motors for ship propulsion (navy frigates, cruise ships, medium size cargo vessels and ice breakers). The application of PM electric motors includes:

- Industry:
 - Industrial drives, e.g., pumps, fans, blowers, compressors, centrifuges, mills, hoists, handling systems, etc.
 - Machine tools.
 - Servo drives.
 - Automation processes.
 - Internal transportation systems.
 - Robots.

- Public life:
 - Air conditioning systems
 - Catering equipment
 - Coin laundry machines
 - Auto-bank machines
 - Automatic vending machines
 - Money changing machines
 - Ticketing machines
 - Bar-code readers at supermarkets
 - Environmental control systems
 - Amusement park equipment
 - Clocks.

- Domestic life:
 - Kitchen equipment (refrigerators, microwave ovens, mixers, dishwashers, etc.)
 - Bathroom equipment (shavers, hair dryers, tooth brushes, massage apparatus)
 - Washing machines and clothes dryers
 - Heating and air conditioning systems
 - Vacuum cleaners
 - Lawn mowers
 - Swimming pool pumps
 - Toys
 - Vision and sound equipment
 - Security systems (automatic garage doors, automatic gates)

- Information and office equipment:
 - Computers
 - Printers
 - Plotters
 - Scanners
 - Facsimile machines
 - Photocopiers
 - Audiovisual aids

- Automobiles with combustion engines.

- Transportation:
 - Elevators and escalators
 - People movers
 - Light railways and streetcars (trams)
 - Electric road vehicles
 - Aircraft flight control surface actuation
 - Electric ships
 - Boats

- Aerospace:
 - Rockets
 - Space shut
 - Satellites

- Medical and healthcare equipment:
 - Dentist's drills
 - Electric wheelchairs
 - Air compressors
 - Trotters
 - Rehabilitation equipment
 - Artificial heart motors

- Power tools:
 - Drills
 - Hammers
 - Screwdrivers
 - Grinders
 - Polishers
 - Saws
 - Sanders
 - Sheep shearing hand pieces

- Renewable energy systems

- Research and exploration equipment

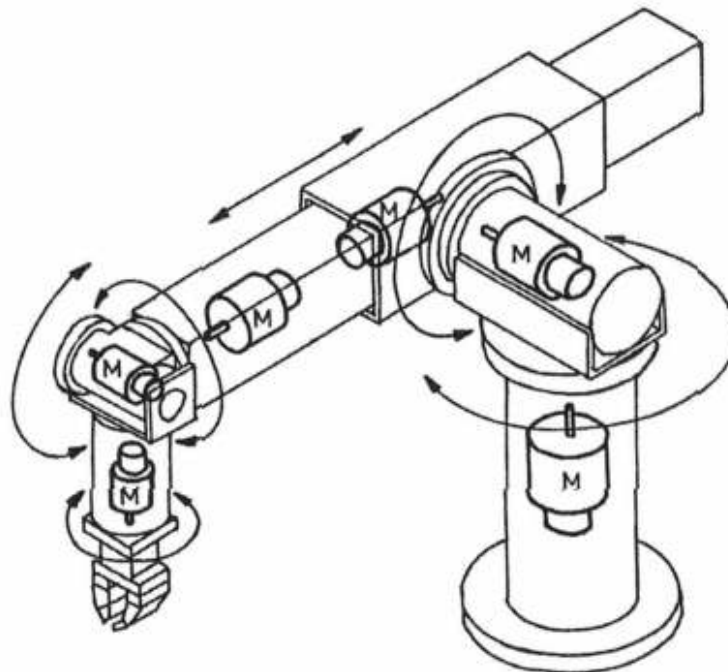


Fig 1.4: An industrial robot (M - electric motor)

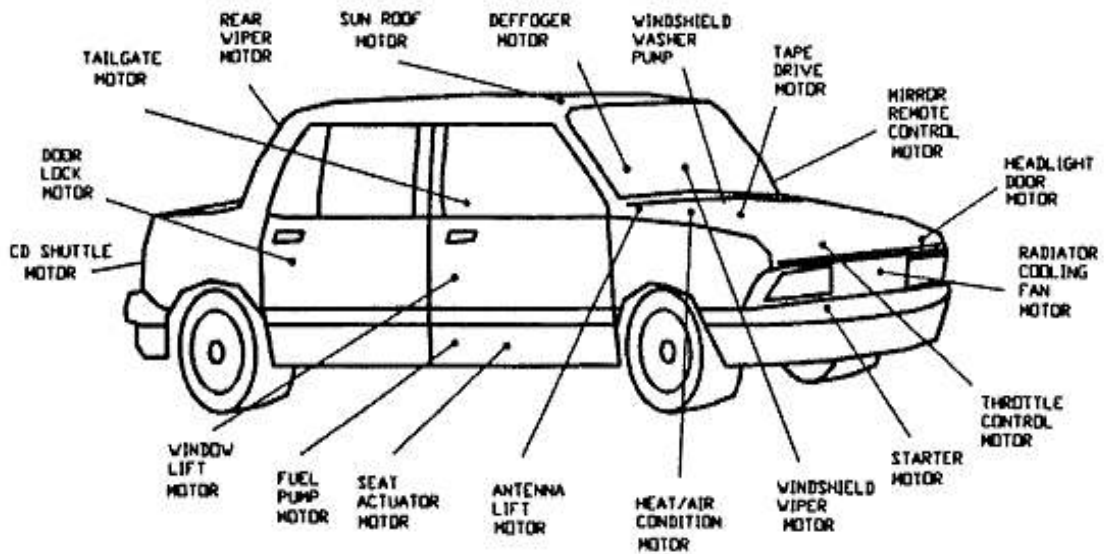


Fig 1.5: PM motors installed in a car

1.6 Previous Study:

PM motor drives have been a topic of interest for the last twenty years. Different authors have carried out modeling and simulation of such drives.

In 1986 Sebastian, T., Slemon, G. R. and Rahman, M. A. reviewed permanent magnet synchronous motor advancements and presented equivalent electric circuit models for such motors and compared computed parameters with measured parameters. Experimental results on laboratory motors were also given.[2]

In 1997 Jang-Mok, K. and Seung-Ki, S, proposed a novel flux-weakening scheme for a Permanent Magnet Synchronous Motor (PMSM). It was implemented based on the output of the synchronous Proportional Integral (PI) current regulator reference voltage to Pulse Width Modulation (PWM) inverter. [6]

The on-set of flux weakening and the level of the flux were adjusted inherently by the outer voltage regulation loop to prevent the saturation of the current regulator.

Attractive features of this flux weakening scheme included no dependency on the machine parameters, the guarantee of current regulation at any operating condition, and smooth and fast transition into and out of the flux weakening mode.

Experimental results at various operating conditions including the case of detuned parameters were presented to verify the feasibility of the proposed control scheme.

1.7 History of PM:

The first PM excitation system was applied to electrical machine as early as the 19th century, e.g. J. Henry (1831), H. Pixii (1832), W. Ritchie (1833), F. Watkins (1835), T. Davenport (1837), M.H. Jacobi (1839).

1.8 Table of Cost

Table 1.1: Cost of the project

Description	Price (NIS)
Hi-Silicon sheets	150
Lathing the stator	350
Cutting Hi-Silicon sheets	150
Copper windings	50
Permanent Magnets & cutting them	100
Lathe the rotor & body	200
The project printing	100
Others	200
TOTAL	1300

1.9 Time Plan:

Time of project is scheduled on 16 weeks Table 1.2 shows how the work is scheduled over these weeks.

Table 1.2: Time plan of the project

Tasks	Weeks	1	3	5	7	9	11	13	15
		2	4	6	8	10	12	14	16
Getting materials		■							
Stator Construction				■	■	■	■		
Rotor Construction						■	■	■	
Testing and operation							■	■	■
Documentation						■	■	■	

CHAPTER TWO

AC MOTOR CLASSIFICATION

2.1 Single-phase PM AC Motor

2.1.1 Single-phase Synchronous Motors

2.1.2 Single-phase Induction Motors

2.2 Reluctance Motor

CHAPTER TWO

AC MOTOR CLASSIFICATION

2.1 Single-phase PM AC Motor:

The single-phase permanent magnet AC motor, acting as conventional synchronous type motor, has found renewed interest in the last two decades. The recent development of high energy magnets has enhanced their application in wide range of areas. The built-in of permanent magnets in the rotor core of synchronous motors as an excitation, and in particular the use of samarium-cobalt or neodymium-boron-iron magnets has challenged innovations in the permanent magnet synchronous motor design and analysis [5].

2.1.1 Single-phase Synchronous Motors:

There are two types of synchronous motors namely reluctance and hysteretic motors. They are simple in construction since they do not require DC field excitation, nor use permanent magnets.

The single-phase synchronous reluctance motor is similar to the induction motor except that some saliency is introduced in the rotor structure by removing some rotor teeth at appropriate places to provide the required number of poles. The reluctance motor can start as an induction motor because the rotor has a squirrel-cage construction. The stator of the reluctance motor has a main winding and an auxiliary winding. This motor starts as an induction motor and at about 75% of synchronous speed the auxiliary winding is disconnected. The motor continues to speed up as a single-phase motor with the main winding connected. When the speed is close to synchronous speed the rotor tends to align itself with the synchronously rotating

forward air gap flux wave and then pulls into synchronism and continues rotating at synchronous speed. The advantages of such motors are that they are brushless and have no dc field winding and are low cost. However, this motor is relatively bulky.

The hysteresis motor uses the hysteresis property of magnetic materials to produce torque. The stator windings are distributed windings that produce a sinusoidal space distribution of flux, while the rotor has a ring of special magnetic material mounted on a cylinder of nonmagnetic material. The stator winding is of the capacitor-run type that makes the stator a nearly balanced two-phase system and produces a rotating field at synchronous speed when excited with a single-phase supply. The revolving field induces eddy-currents in the rotor, and because of hysteresis, the magnetization of the rotor lags behind the induced rotating field [3].

The displaced angle between the stator and rotor fluxes is independent of rotor speed, but depends on the hysteresis loop. Consequently, a constant torque is developed up to synchronous speed. As the rotor reaches synchronous speed, the relative motion between rotor and stator's field decreases, and the frequency of eddy currents decreases. At synchronous speed, the rotor materials become permanently magnetized in one direction. The hysteresis motor has a constant torque-speed characteristic. It is a quiet and smooth-running motor because of the smooth periphery of the rotor cylinder [1].

2.1.2 Single-phase Induction Motors:

These motors are probably the simplest and most rugged of all electric motors. They consist of two basic electrical assemblies: the wound stator and the rotor assembly.

The rotor consists of laminated, cylindrical iron cores with slots for receiving the conductors. On early motors, the conductors were copper bars with ends welded to copper rings known as end rings. Viewed from the end, the rotor assembly resembles a squirrel cage; hence the name squirrel- cage motor is used to refer to induction

motors. In modern induction motors, the most common type of rotor has cast-aluminum conductors and short-circuiting end rings. The rotor turns when the moving magnetic field induces a current in the shorted conductors. The speed at which the magnetic field rotates is the synchronous speed of the motor: [2]

$$n_s = \frac{120 * f}{p} \quad (2.1)$$

Where: n_s : synchronous speed
 f : frequency
 p : number of poles

Synchronous speed is the absolute upper limit of motor speed. At synchronous speed, there is no difference between rotor speeds and rotating field speed, so no voltage is induced in the rotor bars, hence no torque is developed. Therefore, when running, the rotor must rotate slower than the magnetic field. The rotor speed is just slow enough to cause the proper amount of rotor current to flow, so that the resulting torque is sufficient to overcome windage and friction losses, and drive the load. This speed difference between the rotor and magnetic field, called slip, is normally referred to as a percentage of synchronous speed: [2]

$$s = \frac{100 (n_s - n)}{n_s} \quad (2.2)$$

Where: s = slip
 n_s = synchronous speed
 n = actual speed

2.2 Reluctance Motor:

The variable reluctance motor is based on the principle that an unrestrained piece of iron will move to complete a magnetic flux path with minimum reluctance, the magnetic analog of electrical resistance.

If the rotating field of a large synchronous motor with salient poles is de-energized, it will still develop 10 or 15% of synchronous torque. This is due to variable reluctance throughout a rotor revolution. There is no practical application for a large synchronous reluctance motor. However, it is practical in small sizes.

If slots are cut into the conductor less rotor of an induction motor, corresponding to the stator slots, a synchronous reluctance motor results. It starts like an induction motor but runs with a small amount of synchronous torque. The synchronous torque is due to changes in reluctance of the magnetic path from the stator through the rotor as the slots align. This motor is an inexpensive means of developing a moderate synchronous torque. Low power factor, low pull-out torque, and low efficiency are characteristics of the direct power line driven variable reluctance motor. Such was the status of the variable reluctance motor for a century before the development of semiconductor power control [3].

CHAPTER THREE

MOTOR DESIGN

3.1 Introduction

3.2 Rotor Parameter

3.2.1 Differential Rotor MMF and Permeance

3.2.2 Differential Air-Gap Permeance

3.2.3 Calculation of Reluctance Torque

3.2.4 Calculation of Peak Rotor Flux

3.3 Rest Position of the Rotor (θ_0)

3.4 Calculation of Stator Inductance

3.4.1 Simplification of Stator Magnetic Circuit

3.4.2 Fringing Flux Calculation

3.4.3 Stator-Inductance Expression

CHAPTER THREE

MOTOR DESIGN

3.1 Introduction:

Single-phase permanent-magnet (SPPM) synchronous motors of the type shown in Fig. 1.1 have found growing applications especially in low-power household appliances. Because it is well suited to mass production purposes and has a simple construction, and has a cost advantage [1].

Like all PM motors, if the motor is self-starting, problems arise. Starting behavior is dependent on the initial position of the rotor, on the load inertia and the frictional load. And it is shown to be dependent on the electrical parameters, especially on the phase of the stator voltage at the switching instant [5].

At starting, the motor may rotate in either direction. Therefore, the applications are limited to loads, which are not sensitive to direction of rotation.

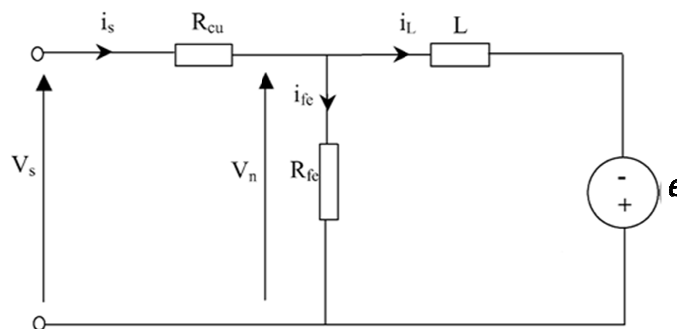


Fig. 3.1: Electrical equivalent circuit of an SPPM motor

The first thing one needs is an accurate enough model to describe the behavior of the motor. At usual synchronous machine, the electrical circuit model may be used for

analysis of the performance, in the form given in Fig. 3.1, along with the mechanical equations. In Fig. 3.1, the resistance R_{fe} is employed to the core losses [1].

Considering the electrical equivalent circuit in Fig. 3.1, equations of the motor may be written as follows:

$$iL = \frac{1}{L} \int (V_n + e) dt$$

$$V_n = V_s - i_s R_{cu}$$

$$i_s = i_L + i_{fe}$$

$$i_{fe} = \frac{V_n}{R_{fe}} \quad (3.1)$$

Where: R_{fe} : the resistance corresponding to core losses
 V_n : rated voltage
 V_s : the supply voltage with a frequency of w and phase angle ε at the switching instant
 R_{cu} and L : resistance and inductance of the stator winding.

And the mechanical equation: [1]

$$J\ddot{\theta} = Ni \Phi_{rp} \sin \theta - T_{rp} \sin[2(\theta - \theta_0)] + T_l \quad (3.2)$$

Where: N : the number of turns of the stator winding
 Φ_{rp} : the peak rotor flux linked by stator winding
 θ : the position of the rotor (angle between rotor and stator axis)
 θ_0 : the initial position of the rotor
 J : the moment of inertia of the rotor and the load
 T_{rp} : the peak reluctance torque
 T_l : the load torque

In the Back EMF expression ($e = \dot{\theta} N \Phi_{rp} \sin(\theta - \theta_0)$) (3.3)

Note that in (3.1) and (3.2), rotor flux linked by stator winding and reluctance torque are assumed to be sinusoidal function of rotor position (θ). In practice, these

variables do not show such pure variations. It is need to express the electrical and mechanical parameters of the motor in terms of the dimensions of the motor. In terms of dimensions as well as the constraints introduced by requirements like rated torque, efficiency, and the starting performance [1].

3.2 Rotor Parameter:

It is needed to consider the magnetic equivalent circuit of the motor with no stator excitation. In this case, the equivalent circuit is as shown in Fig. 3.2:

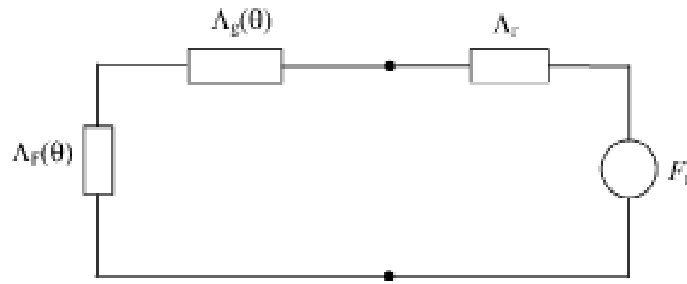


Fig. 3.2: Magnetic equivalent circuit of the rotor of an SPPM motor

In Fig. 3.2, $\Lambda_F(\theta)$ is the stator magnetic circuit permeance and will be neglected here for the make of simplicity. Λ_r represents the rotor permeance as: [1]

$$\Lambda_r = \frac{\mu_p A_m}{l_m} \quad (3.4)$$

Where

μ_p : defined as in Fig. 3.3

A_m : the cross section of the rotor magnet

l_m : represents the mean flux path length in the magnet

F_r is the rotor MMF and is expressed as:

$$F_r = H_c \cdot l_m \quad (3.5)$$

Where

H_c : defined as in Fig. 3.3

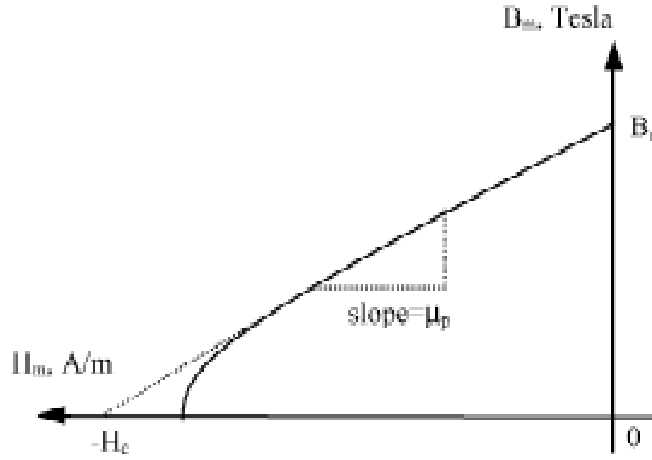


Fig. 3.3: Typical B-H characteristics of a permanent magnet

The rotor MMF is taken to be constant and the variation of the air gap flux with θ is modeled by taking Λ_g to be a function of θ . [3]

$$\Lambda_g(\theta) = \Lambda_{g0} + \Lambda_{g1} \cos 2\theta \quad (3.6)$$

Where $\Lambda_g(\theta)$: the air gap permeance

3.2.1 Differential Rotor MMF and Permeance:

Consider a differential portion of rotor represented by a horizontal differential length dx as shown in Fig. 3.4. It is possible to express the flux path l_m as:

$$l_m = r \cos \theta_s \quad (3.7)$$

Where θ_s : defined with respect to the rotor axis

In Fig. 3.4 and is independent of rotor position, θ ; Therefore, from (3.5), rotor MMF for the section of the rotor becomes: [5]

$$\mathfrak{F}_r(\theta_s) = H_c \cdot r \cdot \cos \theta_s \quad (3.8)$$

Where r : the radius of the rotor

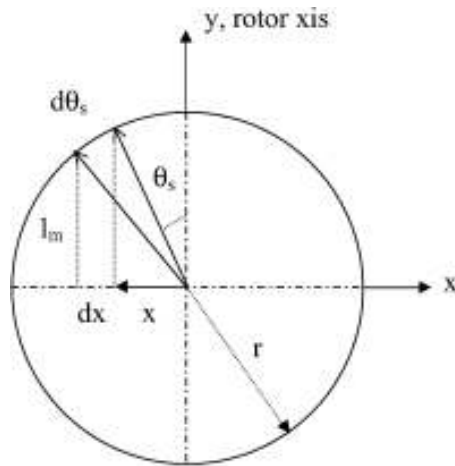


Fig. 3.4: Differential analysis of rotor parameters

To calculate the differential rotor permeance, consider again section of the rotor marked by dx in Fig. 3.4. [1].

$$x = r \sin \theta_s$$

$$dx = r \cos \theta_s d\theta_s \quad (3.9)$$

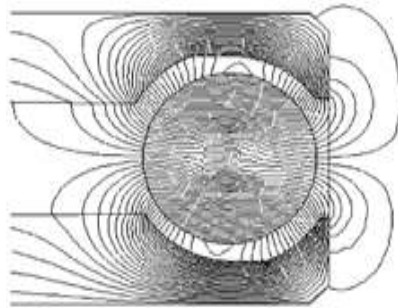


Fig. 3.5: Magnetic field solution results for several rotor positions

$$d\Lambda_r(\theta_s) = \mu_p \frac{dA_m}{l_m} = \mu_p \frac{z_g \cdot dx}{r \cos \theta_s} = \mu_p \cdot Z_g \cdot d\theta_s \quad (3.10)$$

Where Z_g : the axial length of the rotor.

3.2.2 Differential Air-gap Permeance:

Calculation of the variation of $\Lambda_g(\theta)$ is made particularly difficult due to the existence of the fringing field. At this stage, it is wise to consider the variation of the motor magnetic field with angle θ_s , to obtain an idea of how the fringing field changes with position. For this purpose, field solutions of the motor are obtained for different rotor positions.

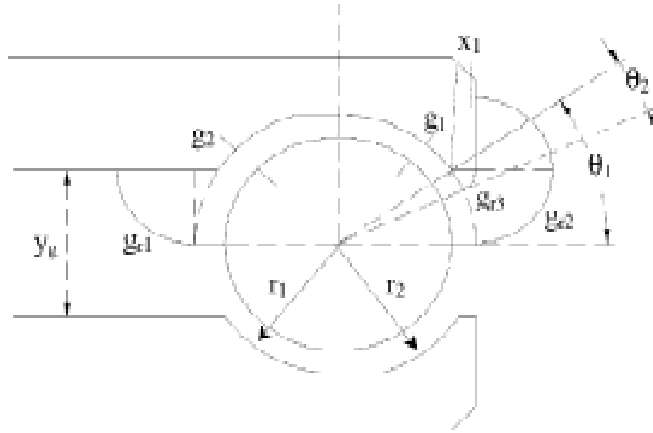


Fig. 3.6: Analysis of air gap permeance density distribution

By studying this figure, it is decided to represent the fringing flux by flux tubes with constant cross section, defined in terms of the dimensions of the motor such as y_g and x_1 as displayed in Fig. 3.6. In defining the tubes, it is assumed their boundary is a fringing flux line defined by a circle. The permeance of the flux tubes on either side of the rotor can now be written in terms of the cross section of the tube (A_i) and their mean flux path length g_{ri} . Lengths of the outer flux lines seen in Fig. 3.6 can be calculated from (3.11)–(3.14). Length of fringing flux lines, g_r is assumed to vary uniformly between the inner and outer gaps of the tubes: [1]

$$g_{r1} = g_2 + \frac{\pi y_g}{4} \quad (3.11)$$

$$g_{r2} = g_1 + \frac{\pi y_g}{4} + \left(r_1 + \frac{y_g}{2} - r_1 \cos \theta_1 - x_1 \right) \frac{\pi}{2} \quad (3.12)$$

$$g_{r3} = g_1 + x_1 \left(\frac{\pi}{2} + \frac{\theta_2}{2} - \theta_1 \right) \quad (3.13)$$

$$g_r = \frac{g_{r1} + g_{r2} + g_{r3}}{3} \quad (3.14)$$

Where:

$$\theta_1 = \sin^{-1} \left(\frac{y_g}{2r_1} \right) \quad (3.15)$$

$$\theta_2 = 2 \sin^{-1} \left(\frac{x_1}{2r_1} \right) \quad (3.16)$$

It is now possible to draw θ_s . Therefore, for a motor with can be expressed as follows:

$$d\Lambda_g(\theta_s) = \mu_0 \frac{Z_g r_g}{g_r} d\theta_s \quad (3.17)$$

Where

θ_s : the differential air gap size with surface angle
 Z_g : differential air gap permeance

$$r_g = r + \frac{g_1 + g_2}{g_r} \quad (3.18)$$

Where

r_g : defined as mean air gap radius

The variation of differential air gap permeance can be visualized in a simplified manner if it is normalized, for example, with respect to the permeance of the small air-gap section. In this case, the differential permeance is only a function of g_1/g_r . In Fig. 3.7 can be used which is the representation of (g_1/g_r) [1].

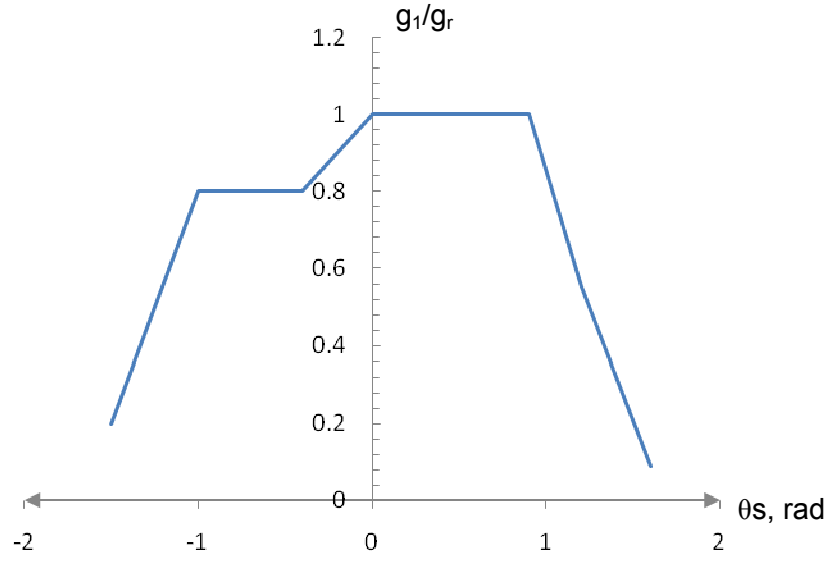


Fig. 3.7: Normalized air gap permeance variation

$$\frac{g_1}{g_r}(\theta_s) = 0.75 + 0.32 \cos(\theta_s - \theta_p) \quad (3.19)$$

$$\theta_p = 0.1068 \text{ rad } (6.12^\circ).$$

Where θ_p : the phase shift of the fundamental component
 θ_s : the variation of the motor magnetic field with angle from $0-2\pi$

Then differential air gap permeance becomes:

$$d\Lambda_g(\theta_s, \theta) = \left(0.75 \frac{\theta_0 Z_g r_g}{g_1} + 0.32 \frac{\theta_0 Z_g r_g}{g_1} \cos 2(\theta_s - \theta_p + \theta) \right) d\theta_s \quad (3.20)$$

Where: Z_g : depth of the motor

Note that in (3.20), the rotation of the rotor is introduced by a phase shift of rotor position (θ) in the ac component.

3.2.3 Calculation of Reluctance Torque:

The reluctance torque can be calculated in terms of magnetic co-energy W_{co} :

$$T_{re} = \frac{dW_{co}}{d\theta} \quad (3.21)$$

the differential co-energy is given by: [1]

$$dW_{co}(\theta_s, \theta) = \frac{1}{2} F_r^2(\theta_s) d\Lambda_{re}(\theta_s, \theta) \quad (3.22)$$

Where

$F_r(\theta_s)$: the rotor MMF

$d\Lambda_{re}$: equivalent differential permeance seen by the rotor

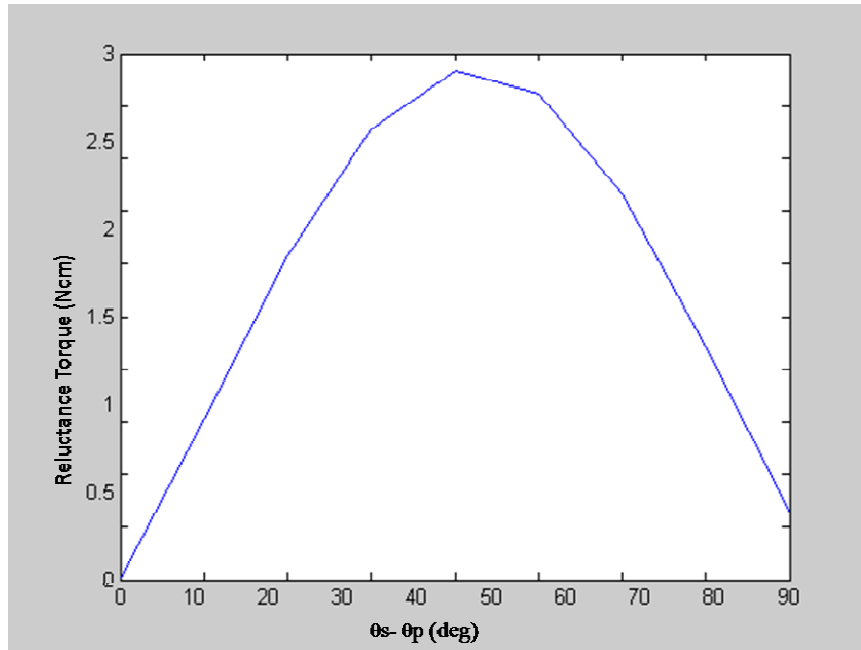


Fig. 3.8: Calculated reluctance torque against position

Considering the magnetic equivalent circuit in Fig. 3.2, $d\Lambda_{re}$ is calculated as follows:

$$d\Lambda_{re}(\theta_s, \theta) = \frac{d\Lambda_r(\theta_s) d\Lambda_g(\theta_s, \theta)}{d\Lambda_r(\theta_s) + d\Lambda_g(\theta_s, \theta)} \quad (3.23)$$

Reluctance torque for any rotor position becomes: [1]

$$T_r(\theta) = \int_{-\frac{\pi}{2}}^{\frac{\pi}{2}} \mathfrak{F}_r^2 d\Lambda'_{re} \quad (3.24)$$

where $d\Lambda'_{re}$ is given by:

$$d\Lambda'_{re} = -2 \frac{c^2 b \sin 2(\theta_s - \theta_p + \theta)}{[c + a + b \cos 2(\theta_s - \theta_p + \theta)]^2} \quad (3.25)$$

With:

$$a = 0.75 \mu_0 z_g \frac{r_g}{g_1} \quad (3.26)$$

$$b = 0.32 \mu_0 z_g \frac{r_g}{g_1} \quad (3.27)$$

$$c = \mu_p z_g \quad (3.28)$$

An important issue is the determination of the rest position. The rest position corresponds to the position of the rotor where rotor flux is maximum.

When the peak-pole flux value is calculated from the previous equations.

3.2.4 Calculation of Peak Rotor Flux:

An approximate of air gap permeance in (3.20) is used for the calculation of peak rotor flux. Therefore, for this calculation the actual air-gap permeance variation needs to be considered. Since peak rotor flux is of interest here, the rest position of rotor where flux is maximum. The rotor flux linked by the stator winding is assumed to be sinusoidal function of rotor position (θ) as in (3.1) and (3.2) [1, 3].

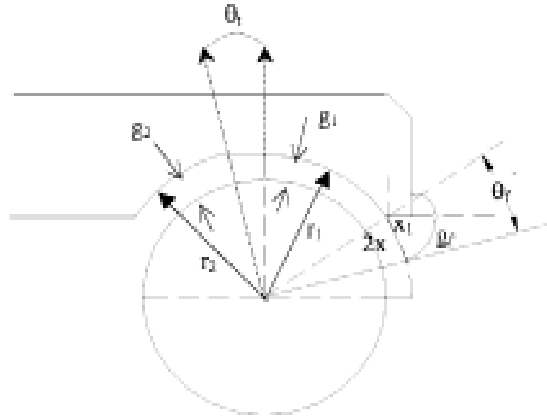


Fig. 3.9: Representation of the fringing field at the rest position

As field lines of the test motor for the rest position in Fig. 3.5 is investigated it is observed that the fringing field is important only in the region adjacent to the smaller air gap. It is essential to take into account the effect of this fringing field to determine the peak flux with acceptable accuracy. The angle θ_f in Fig 3.9 can be represented as follows: [1]

$$\theta_f = 2 \sin^{-1} \left(\frac{x_1}{r_1} \right) \quad (3.29)$$

The length of the outermost flux line g_f can be calculated from:

$$g_f = g_1 + 2x_1 \left(\frac{\pi}{2} + \frac{\theta_f}{2} - \theta_2 \right) + x_1 \frac{\pi}{2} \quad (3.30)$$

where g_1 : the length of small air gap

To simplify the handling of the problem, the magnetic circuit around the rotor can be represented with an equivalent air gap region composed of two uniform air gaps with lengths g_1 and g_2 . Such a representation is shown in Fig. 3.10. In this Fig., the transition region, represented with the angle θ_i in Fig. 3.9, is equally included in both uniform air gap regions of (g_1) and (g_2), and the fringing field effect is represented by extending the constant air gap region (g_1), by an angle θ_{fe} . θ_{fe} is calculated from

(3.31), which is determined so as to give the same permeance as the actual fringing region (a linear variation is assumed between g_1 and g_f) [1].

$$\theta_{fe} = \frac{\theta_f}{2} \left(1 + \frac{g_1}{g_f} \right) \quad (3.31)$$

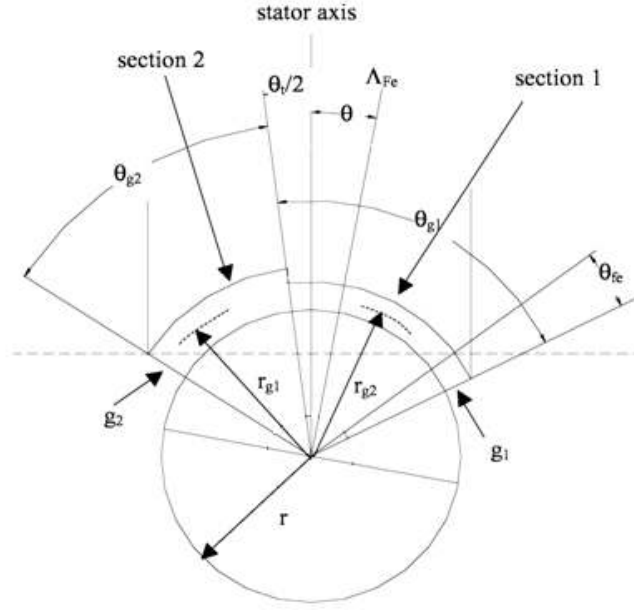


Fig. 3.10: Equivalent rotor shape with uniform air-gaps

Now the air gap has two sections as shown in Fig. 3.10 where r_{g1} and r_{g2} are the mean radiuses of the respective sections. The differential permeance of the sections are then calculated as follows, for Section 1: [1, 5]

$$d\Lambda_{g1}(\theta_s) = \mu_0 \frac{r_{g1} z_g}{g_1} d\theta_s \quad (3.32)$$

Similarly, for Section 2:

$$d\Lambda_{g2}(\theta_s) = \mu_0 \frac{r_{g2} z_g}{g_2} d\theta_s \quad (3.33)$$

Then determining the flux crossing the air gap. Considering the magnetic equivalent circuit given in Fig. 3.2, for the section of the rotor facing air-gap Section 1, the equivalent differential permeance becomes: [1, 3]

$$d\Lambda_{re1}(\theta_s) = \frac{d\Lambda_0(\theta_s)d\Lambda_{g1}(\theta_s)}{d\Lambda_0(\theta_s)+d\Lambda_{g1}(\theta_s)} \quad (3.34)$$

And for Section 2:

$$d\Lambda_{re2}(\theta_s) = \frac{d\Lambda_0(\theta_s)d\Lambda_{g2}(\theta_s)}{d\Lambda_0(\theta_s)+d\Lambda_{g2}(\theta_s)} \quad (3.35)$$

Total flux linking the stator coil is calculated from:

$$\Phi = \int \mathfrak{I} d\Lambda \quad (3.36)$$

Therefore, considering Fig. 3.10, rotor flux linked by stator winding is calculated as follows:

$$\Phi_r(\theta) = \int_{-(\theta_{g1}-\frac{\theta_t}{2}-\theta)}^0 \mathfrak{I}_0(\theta_s)d\Lambda_{re1}(\theta_s) + \int_0^{(\theta_{g2}-\frac{\theta_t}{2}-\theta)} \mathfrak{I}_0(\theta_s)d\Lambda_{re2}(\theta_s) \quad (3.37)$$

Where: θ : the position of the rotor and
 Φ_{rp} : should be calculated for $\theta = \theta_0$. In (3.37)

The second and third components correspond to the contribution of the section of the rotor. Some values of Φ_{rp} calculated from (3.37) for several values of rotor position (θ) are shown: [1, 2]

3.3 Rest Position of the Rotor (θ_0):

If there is no stator excitation, the rotor stills in a position where the permeance of the magnetic circuit is maximum. Knowing this position is important for redicting the starting behavior of the motor with acceptable accuracy. In calculating the initial (rest) position of the rotor, the position of the rotor at which there is minimum (zero) reluctance torque or maximum flux in the air gap.

Although several approaches with varying degree of accuracy has been experimented with. In other words, it is assumed that the permeance of the air gap alone determines the rest position.

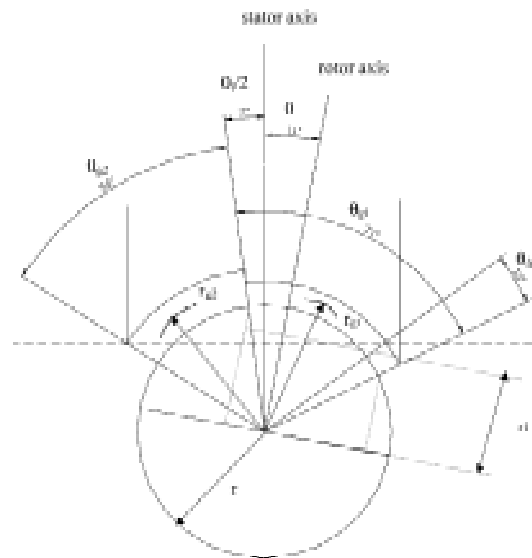


Fig. 3.11: Equivalent rotor shape with uniform air-gaps for the rest position calculation

Consider the equivalent rotor shape with two uniform air gaps given in Fig. 3.11, whose permeance expression derivation is explained in the previous section. The MMF on the surface of the rotor may be viewed as to be proportional to the mean flux path in the rotor magnet. For example, for the section of the rotor facing the small air gap region (g_1) the mean flux path l_{r1} in Fig. 3.11 in the rotor can be calculated as: [3]

$$\begin{aligned}
l_{r_1} &= \frac{\int_{-\left(\frac{\theta_t}{2}+\theta\right)}^{\left(\theta_{g_1}-\frac{\theta_t}{2}-\theta\right)} r \cos \theta \, d\theta}{\theta_{g_1}} \\
&= r \frac{\sin\left(\theta_{g_1}-\frac{\theta_t}{2}-\theta\right)+\sin\left(\frac{\theta_t}{2}+\theta\right)}{\theta_{g_1}}
\end{aligned} \tag{3.38}$$

Then, the equivalent MMF on the rotor surface facing Section1 becomes:

$$\mathfrak{F}_{s_1} = H_k \cdot l_{r_1} \tag{3.39}$$

Where H_k : the average operating magnetic flux intensity of the rotor.

The permeance of the air gap region (Section 1) in Fig 3.10, for a unit axial length of the rotor is:

$$\Lambda_{g_1} = \mu_0 \frac{r_{g_1} r_{g_2}}{g_1} \tag{3.40}$$

Then, the flux crossing the air gap in the considered section is given by the following equation:

$$\begin{aligned}
\Phi_{g_1} &= \mathfrak{F}_{s_1} \Lambda_{g_1} \\
&= H_k r \mu_0 \frac{r_{g_1}}{g_1} \left[\sin\left(\theta_{g_1} - \frac{\theta_t}{2} - \theta\right) + \sin\left(\frac{\theta_t}{2} + \theta\right) \right]
\end{aligned} \tag{3.41}$$

In the same way, with changing parameters, the air-gap flux of the uniform gap region (g_2) is obtained as follows:

$$\Phi_{g_2} = H_k r \mu_0 \frac{r_{g_2}}{g_2} \left[\sin\left(\theta_{g_2} + \frac{\theta_t}{2} + \theta\right) - \sin\left(\frac{\theta_t}{2} + \theta\right) \right]. \tag{3.42}$$

The total air-gap flux is:

$$\phi_g = \phi_{g_1} + \phi_{g_2}. \quad (3.43)$$

The position at which the air-gap flux has its maximum value is the rest position of the rotor and can be found by solving (3.44) for θ :

$$\frac{d\phi_g}{d\theta} = 0 \quad (3.44)$$

From (3.42), the rest position of the rotor is calculated from:

$$\frac{\sin\left(\frac{\theta_{g1} - \theta_t}{2} - \theta_0\right)}{\sin\left(\frac{\theta_{g2} + \theta_t}{2} + \theta_0\right)} = \frac{\Lambda_2}{\Lambda_1} = \frac{g_1 r_{g2} \sin(\theta_{g2}/2)}{g_2 r_{g1} \sin(\theta_{g1}/2)} \quad (3.45)$$

3.4 Calculation of Stator Inductance:

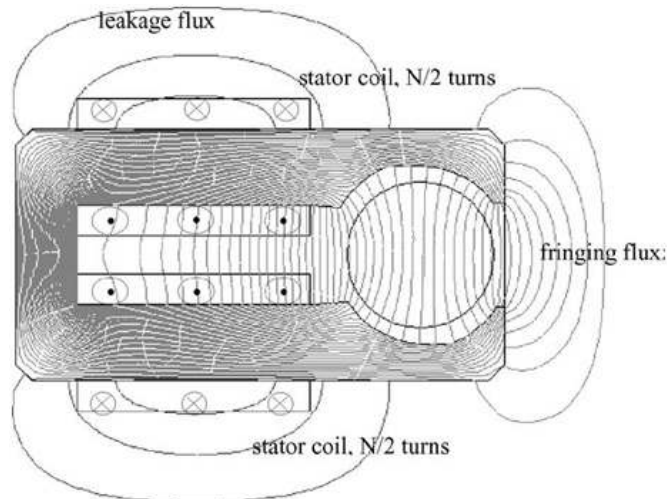


Fig. 3.12: Field distribution just for stator excitation

For the calculation of the inductance of the stator coil it is essential to consider the three-dimensional (3-D) field distribution. This is because the air gap, as seen by the stator coil, is very large (permanent magnet rotor has very low permeability) and the leakage and fringing flux becomes important. Fig. 3.12 is the magnetic equivalent circuit of the motor when only the stator is excited. [1]

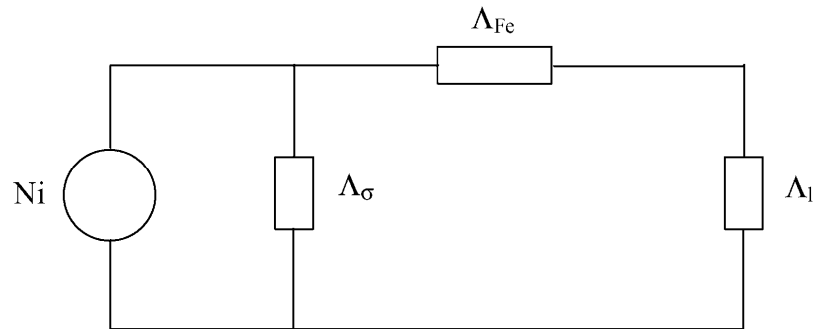


Fig. 3.13: Magnetic equivalent circuit for stator excitation

In Fig. 3.13, Λ_{Fe} is the permeance of the stator core and is neglected since the flux densities in the core are very low. Λ_l parallel core section embracing the rotor, is the permeance of the air gap between the stator legs including the fringing flux between the stator legs. Λ_σ is the permeance of the leakage path outside the stator legs, flux bulging out between stator legs and will be neglected. Ni is the MMF of the stator excitation where i : is the stator winding current. [5]

3.4.1 Simplification of Stator Magnetic Circuit:

Magnetic circuit of a SPPM motor is shown in Fig. 3.12. The variable dimensions of the air gap make the calculation of the permeance of the space between stator legs unnecessarily complicated. Since the distance between the legs is quite large, a simplification in the details is possible without losing accuracy. For this purpose, first the transition region between the sections with air gaps g_1 and g_2 is divided into two equal parts and the stepped air-gap geometry in Fig. 3.14 is obtained. [1]

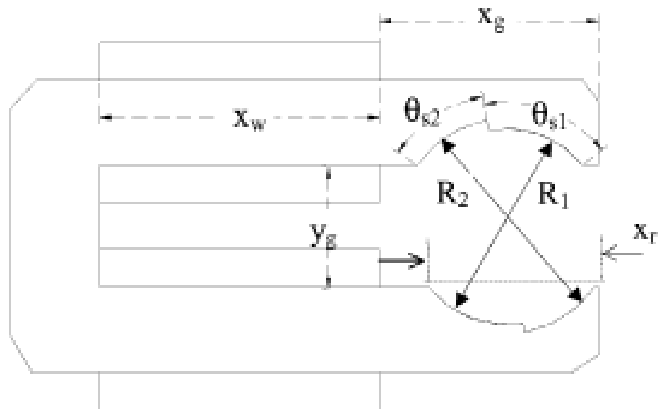


Fig. 3.14: Magnetic circuit of the stator with a stepped-air gap

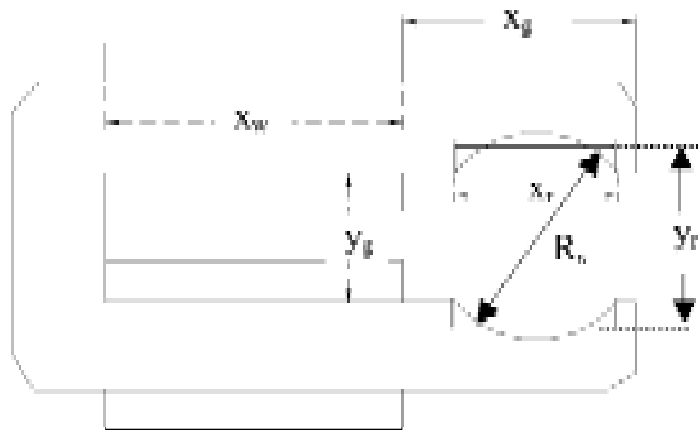


Fig. 3.15: Stator magnetic circuit with simplified rotor gap

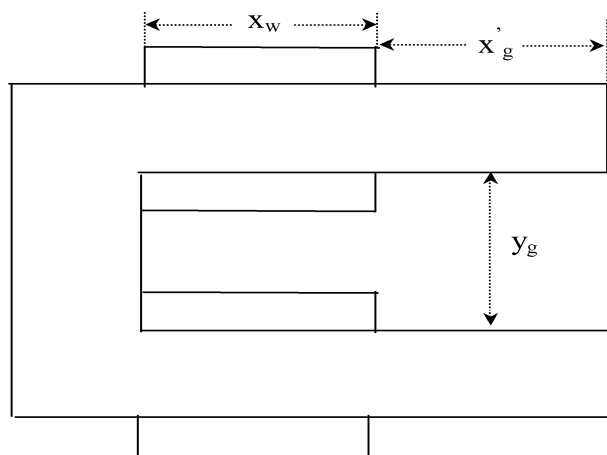


Fig. 3.16: Simplified magnetic circuit of the stator

A further simplification is made by replacing the stepped air gap geometry with a equivalent geometry as in Fig. 3.16 so as to give the same permeability. For this purpose, the following actions are taken. First, the air gap is replaced with an equivalent unstepped geometry in Fig. 3.15 whose radius, R_s :

$$R_s = \frac{\theta_{s1}R_1 + \theta_{s2}R_2}{\theta_{s1} + \theta_{s2}} \quad (3.46)$$

Where R_1 and R_2 are defined as in Fig. 3.14. The unstopped geometry is replaced with an equivalent rectangular geometry with air-gap length, y_r in Fig. 3.15 where:

$$\theta_s = \cos^{-1} \left(\frac{y_g}{R_s} \right) \quad (3.47)$$

$$y_r = \frac{R_s \sin \theta_s}{\theta_s} \quad (3.48)$$

Finally, this rectangular geometry is replaced with another rectangular geometry in Fig. 3.16 with air gap length of y_g , the actual length between the parallel sections of the stator legs in Fig. 3.14. Now, the resulting width, x_g of the part of the stator core not bearing the excitation coil seen in Fig. 3.16 becomes:

$$x'_g = x_g - x_r \left(1 - \frac{y_g}{y_r} \right) \quad (3.49)$$

3.4.2 Fringing Flux Calculation:

Because of the very large distance between the stator legs, flux completing its path outside the magnetic core becomes important. Fig. 3.17(a) is the top view of the stator core showing the fringing regions. Flux paths on the side of the coils and the fringing flux in Fig. 3.12 adjacent to the end of the core is taken into account [1].

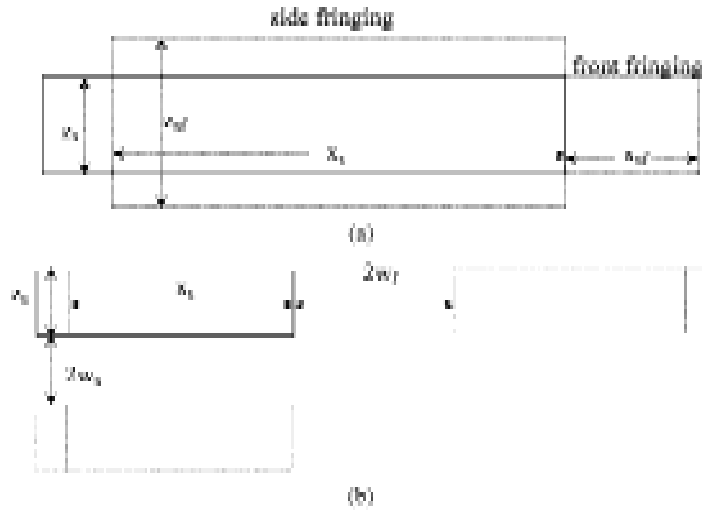


Fig. 3.17: (a) Top view of the stator core with fringing regions
 (b) Approximate model of stator core for fringing calculations

In Fig. 3.17(a) z_s is the actual axial length of the stator core and z_{sf} is the corrected axial length of the core including the effect of the side fringing region. x_s is the width of the stator legs of the simplified geometry and x_{sf} is the extension of the stator core due to the front fringing region. z_{sf} and x_{sf} are determined by assuming similar imaginary structures as seen in Fig. 3.17(b) at a distance $2w_f$ for front fringing and $2w_s$ for side fringing. In this approximate model, determination of the distances w_f and w_s are important. Fringing flux regions of the test motor are analyzed by 3-D field solutions. It is decided to take the values of w_f and w_s as the distances between the points where the fringing flux lines start and the point at which their density is reduced to 1% of the starting value. In this way, it is guaranteed that the imaginary structures has no any magnetic effect on the actual geometry. The distances are determined in terms of motor dimensions as follows: [1]

$$w_s = 2z_s \quad (3.50)$$

$$w_f = 2x_s \quad (3.51)$$

Fringing flux calculation is completed with the application of Carter's method to determine the effective core lengths z_{sf} and x_{sf} follows:

$$z_{sf} = z_s + w_s(1 - \sigma_s) \quad (3.52)$$

$$x_{sf} = w_f(1 - \sigma_f) \quad (3.53)$$

Where, σ is Carter's coefficient and is defined as

$$\sigma_s = \frac{2}{\pi} \left(\tan^{-1} \left(\frac{w_s}{y_g} \right) - \frac{y_g}{2w_s} \ln \left[1 + \left(\frac{w_s}{y_g} \right)^2 \right] \right) \quad (3.54)$$

Where: σ_s : carter's coefficient of stator

$$\sigma_f = \frac{2}{\pi} \left(\tan^{-1} \left(\frac{w_f}{y_g} \right) - \frac{y_g}{2w_f} \ln \left[1 + \left(\frac{w_f}{y_g} \right)^2 \right] \right) \quad (3.55)$$

Where: σ_f : carter's coefficient of fringing

3.4.3 Stator-Inductance Expression:

After the calculations above, the total permeance of the air gap of stator core is evaluated as follows:

$$\Lambda_s = \mu_0 \frac{x_w z_{sf}}{3y_g} \quad (3.56)$$

In (3.56), the first component corresponds to the permeance of the stator core bearing the excitation coil, including side fringing, the second component corresponds to the permeance of the stator core beyond the excitation coil including the side fringing, and the third one covers the permeance of the front fringing region. In the first component, division by 3 comes from the fact that in the corresponding region, flux lines do not link the excitation coil completely [1].

$$\Lambda'_s = \left(\mu_0 \frac{x'_g Z_{sf}}{y_g} + \mu_0 \frac{x_{sf} Z_{sf}}{y_g} \right) \quad (3.57)$$

Then, the inductance is simply calculated from:

$$l = N^2(\Lambda_s - \Lambda'_s) \quad (3.58)$$

CHAPTER FOUR

MOTOR CONSTRUCTION

4.1 Stator

4.2 Rotor

CHAPTER FOUR

MOTOR CONSTRUCTION

4.1. Stator:

This types of motor has special design of stator, classified as non-slotted motor, it is consider as self-starting motor, with a step formed in the part above a rotor that make an additional air gap with a first air gap equals 2 mm, and the second air gap equal 2.5 mm, above the rotor to make air gaps (two non-uniforms air gaps).

Fig 4.1 shows the construction of the stator:



Fig 4.1: Construction of stator

Only an example of one stack of the stator, there are several stacks that are fixed together to construct a laminated stack that is fixed with a bolt to make it more stable. The motor width approximately 4 cm, as shown in Fig 4.2:

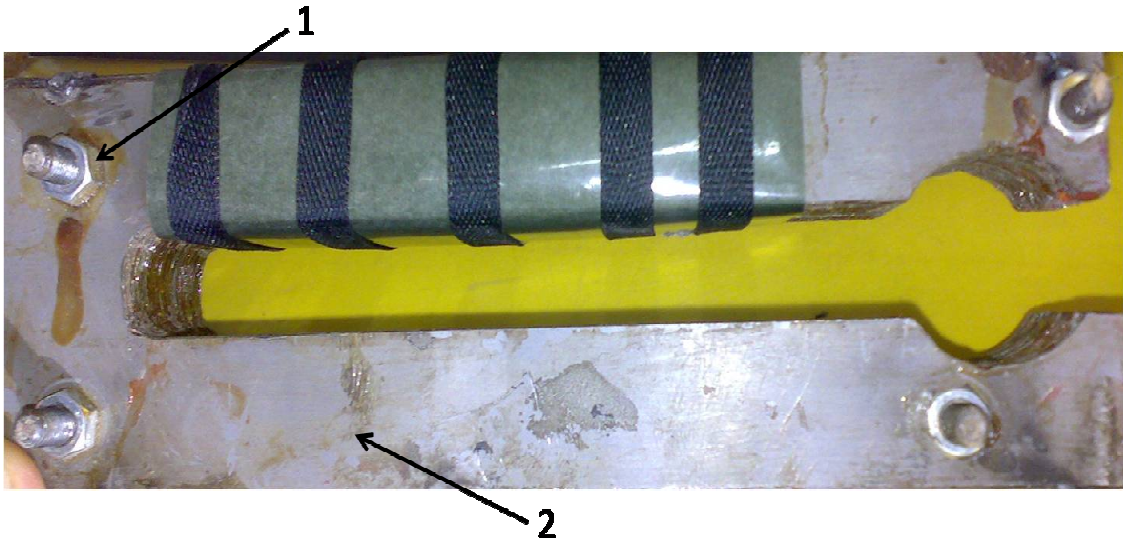


Fig 4.2: Stator (1) bolt(2) stator body

The stack is made from a material called Hi-silicon material which is classified as semi-conductor material, with width equals 3 mm. we chose this type because it has corrosion resistance against the humidity and stain. Hi-silicon increases the maximum magnetic permeability corresponding to critical magnetic field intensity, reduces the area of the hysteresis loop, increases the resistivity, and practically excludes the aging.

In the stator there are winding of electric motors that are made of solid copper conductor wires with round or rectangular cross sections, The electric conductivity at 20°C of copper wires is $57 \cdot 10^6 = \sigma_{20} = 57 \cdot 10^6$ S/m. For aluminum wires $\approx 33 \cdot 10^6$ S/m. The electric conductivity depends on temperature; the equation up to 150°C can be expressed as:

$$\sigma = \frac{\sigma_{20}}{1 + \alpha(\theta - 20)} \quad (4.1)$$

Where: σ : the temperature coefficient of electric resistance,
 For copper wires = 0.00393 1/ °C and for aluminum wires = 0.00403 1/ °C.

The windings formed in the stator as shown in the Fig 4.3 , with number of turns equals approximately 1400 turns in both sides with a resistance $R= 240 \Omega$.

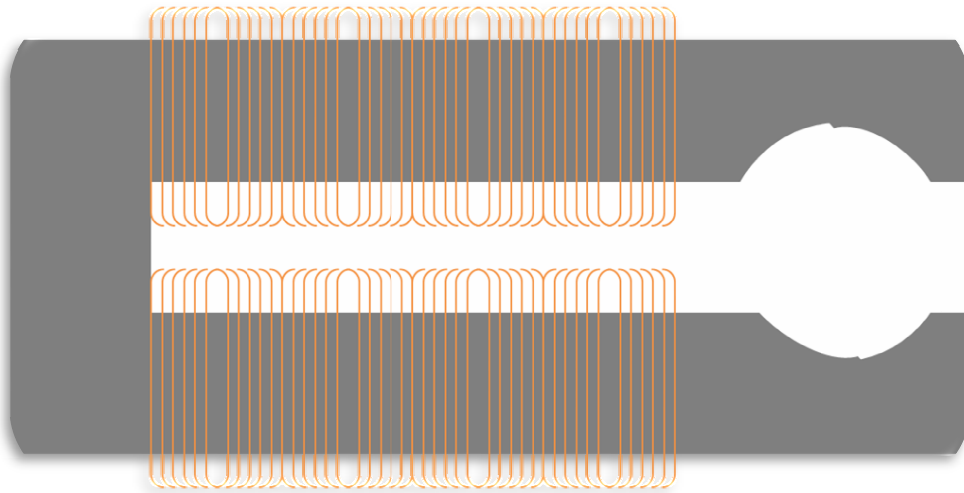


Fig 4.3: Stator windings (drawing)



Fig 4.4: Stator windings (practical)

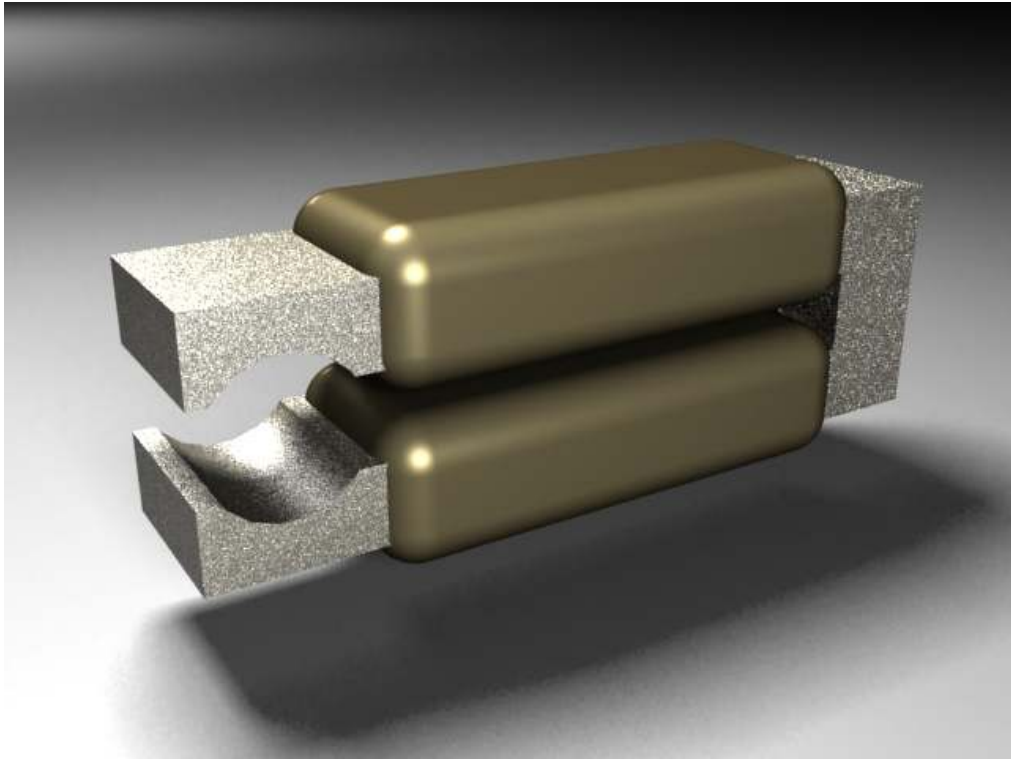


Fig 4.5: Stator design (3dmax)

How the windings are arranged, as shown in Fig 4.6:

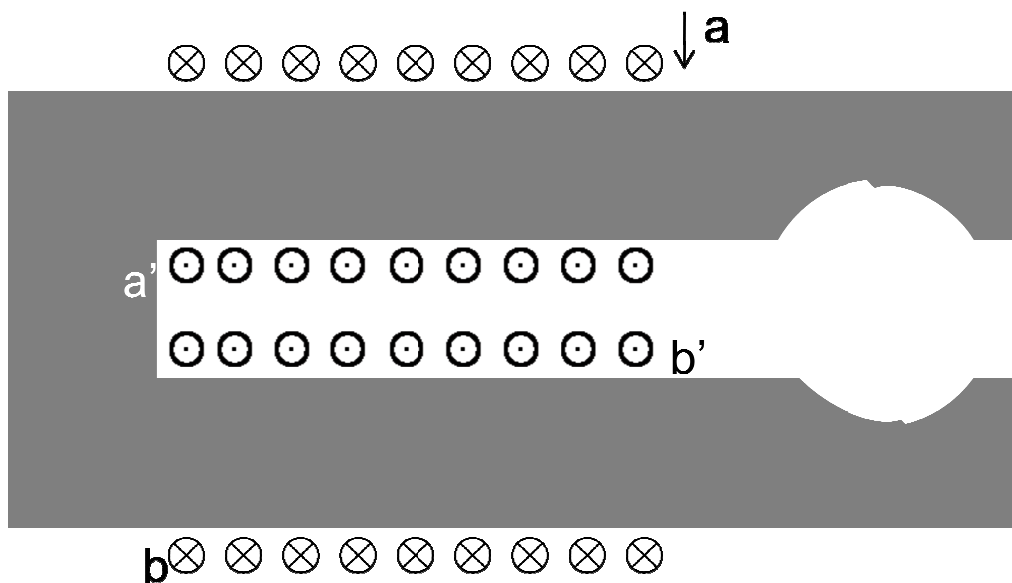


Fig 4.6: (a) starting point of windings (b) ending point of windings (drawing)



Fig 4.7: (a) starting point of windings (b) ending point of windings (practical)

4.2. Rotor:

In the rotor there is a Permanent Magnet (PM) (NdFeB) type. It used because it is susceptible to corrosion, its magnets have great potential for considerably improving the performance-to-cost ratio for many applications. For these reasons it has a major impact on the development and application of PM apparatus.

The rotor is made from iron, for increasing flux density. With the diameter equals 28.5 mm.

To make is better to cut the top of the rotor, to fix the PM above the rotor that has a shape like cylinder, which becomes as a horizontal platform, to fix the horizontal PM with an angle θ more than 120^0 , to help the EMF to distribute uniformly from the surface of PM.

The PM is fixed on the rotor as shown in Fig 4.8:

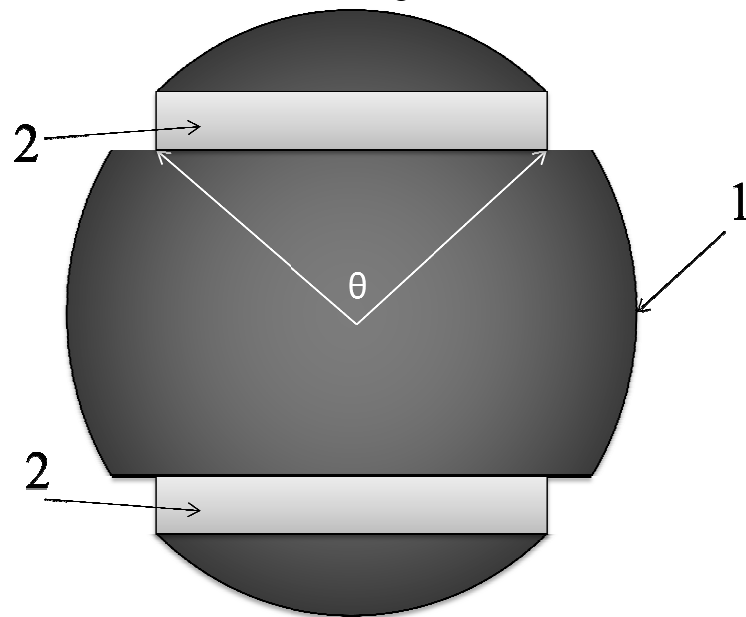


Fig 4.8: Rotor design (1) Rotor (2) Pairs of PM (drawing)

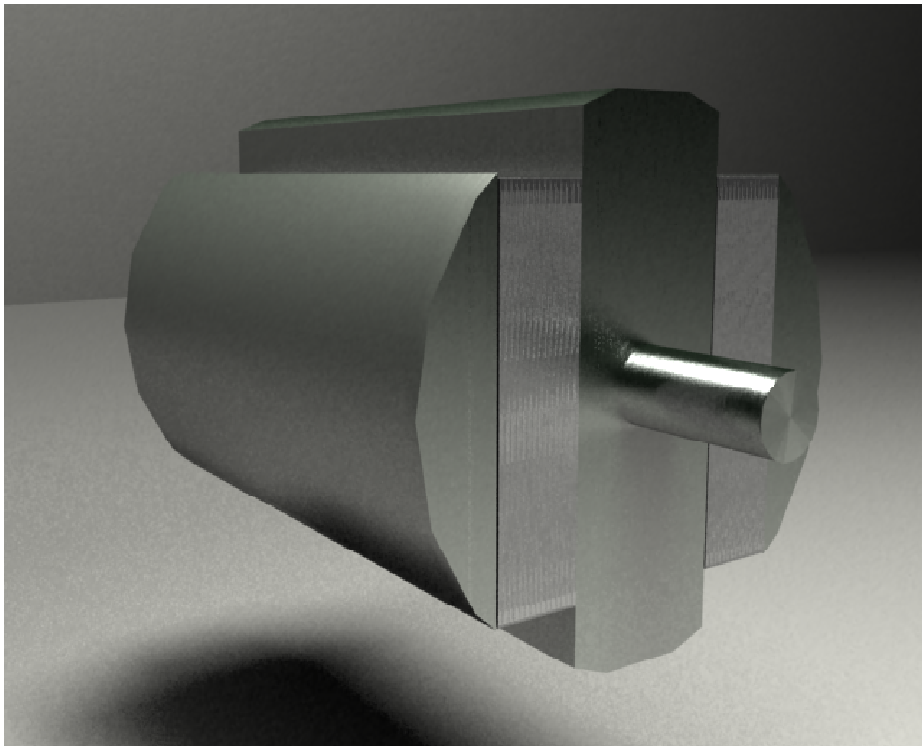


Fig 4.9: Rotor design (3dmax)

After fixing the Pm on the rotor it is just put the rotor shaft on the correct place and make the shape of motor and fixing it on the body of motor and put the bearings for more easier move while moving, the Fig 4.10 show the final construction of the motor.

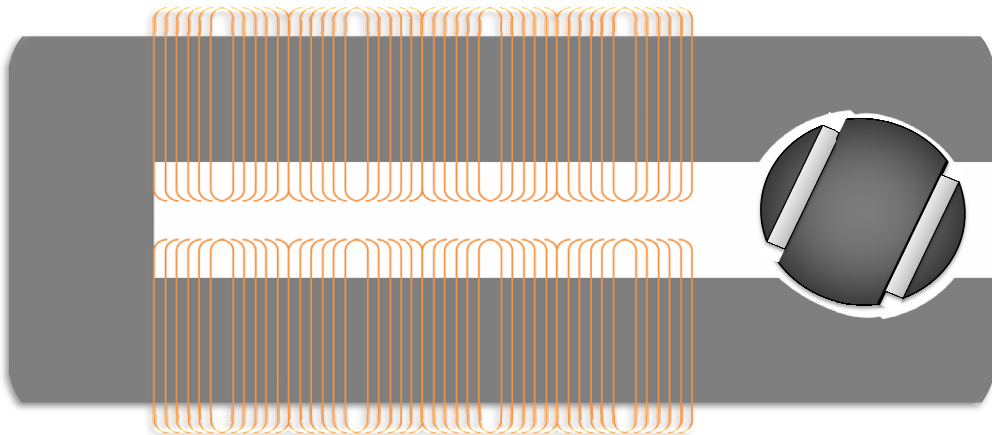


Fig 4.10: Final construction of motor (drawing)

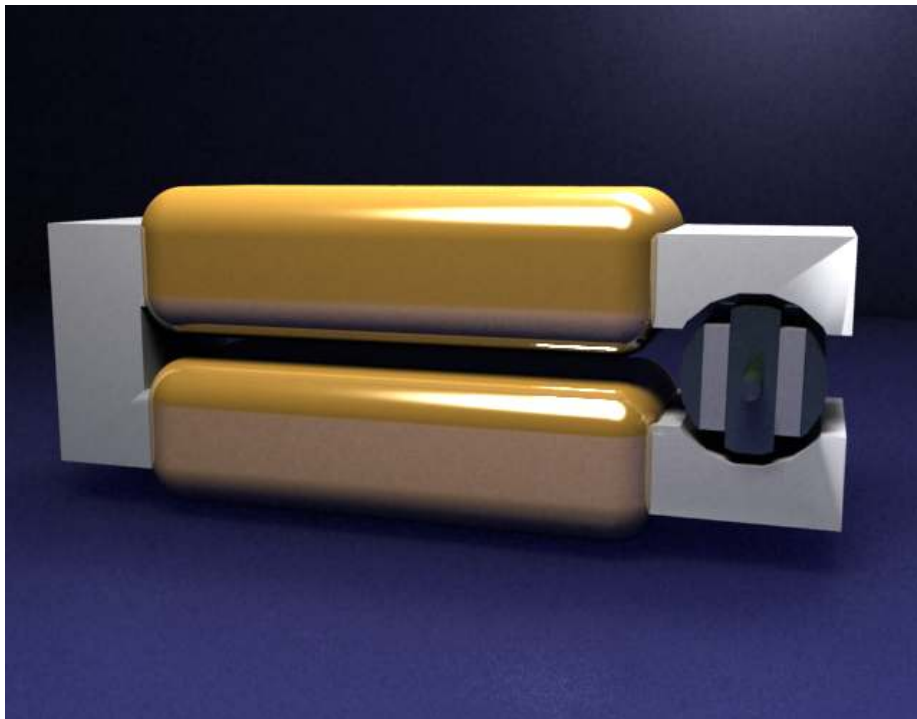


Fig 4.11: Final construction of motor (3dmax)

Catia drawing of the project, as shown in Fig 4.12:

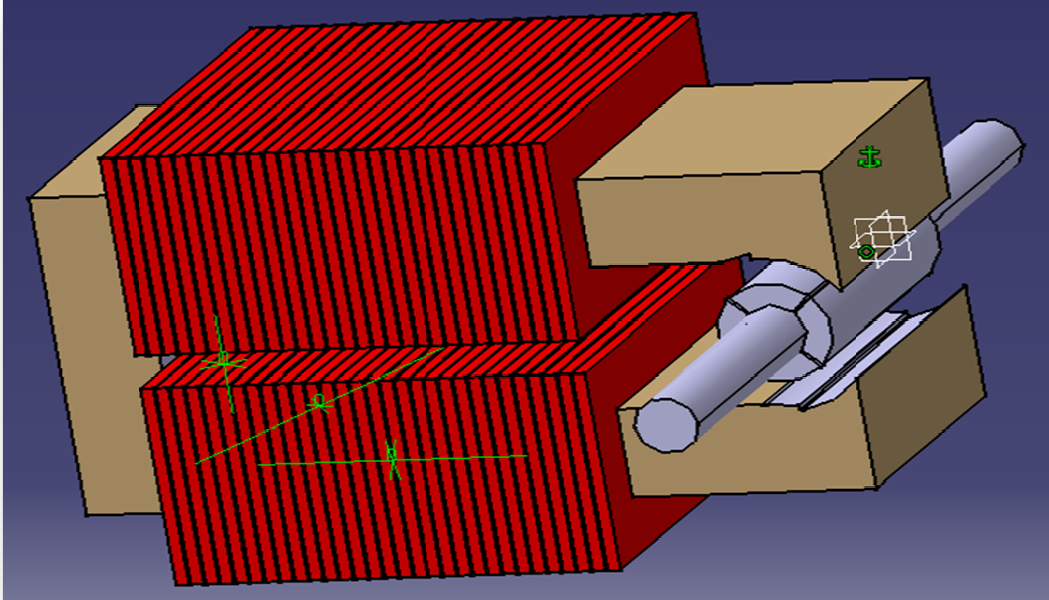


Fig 4.12: Catia drawing of the project (3-D view)

CHAPTER FIVE

SPEED CONTROL

5.1 Speed control of PM motor

5.2 PI controller

5.3 Frequency converter

5.3.1 Frequency converter principles

5.3.2 Variable frequency

CHAPTER FIVE

SPEED CONTROL

5.1 Speed Control of PM Motor:

Many applications such as robotics and factory automation require precise control of speed and position. speed control systems allow one to easily set and adjust the speed of a motor. The control system consists of a speed feedback system, a motor, a frequency converter, a controller and a speed setting device as Tacho Generator (TG). A properly designed feedback controller makes the system insensible to disturbance and changes of the parameters [7].

The purpose of a motor speed controller is to take a signal representing the demanded speed, and to drive a motor at that speed. Closed Loop speed control systems have fast response, but become expensive due to the need of feedback components such as TG.

For a SPPM motor drive system with a full speed range, the system will consist of a motor, a frequency converter, a controller (constant torque and flux weakening operation, generation of reference currents and PI controller) as shown in Fig. 5.1.

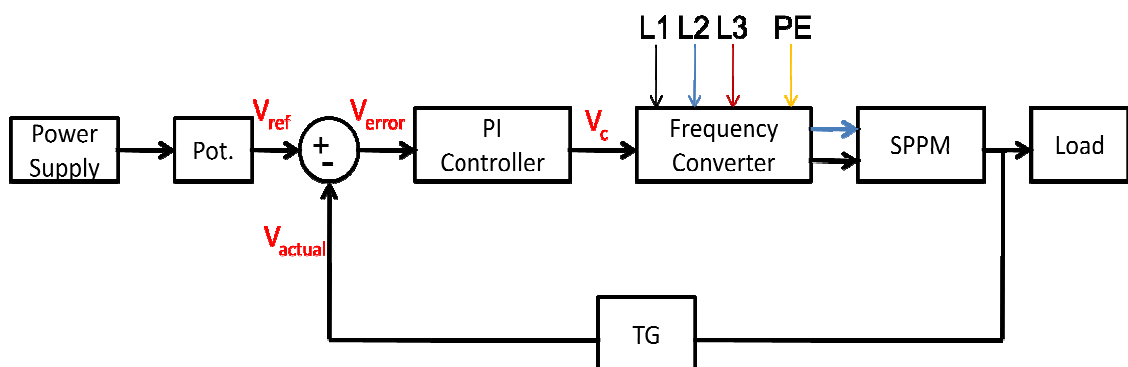


Fig 5.1: Closed loop system of SPPM motor

5.2 PI controller:

Speed controller calculates the difference between the reference speed and the actual speed producing an error, which is fed to the PI controller. PI controllers are used widely for motion control systems. They consist of a proportional gain that produces an output proportional to the input error and an integration to make the steady state error zero for a step change in the input. Block diagram of the PI controller, as shown in Fig 5.2. [6].

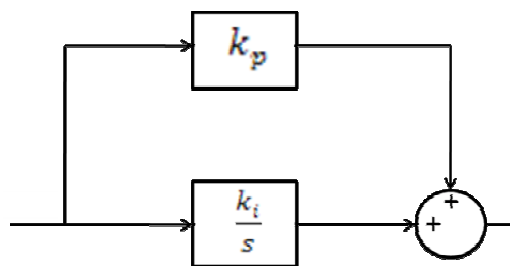


Fig 5.2: PI controller

$$G(s) = k_p + \frac{k_i}{s} \quad (5.1)$$

Where: k_p : proportional constant
 K_i : integral constant

s is defined as steady-state condition for the system.

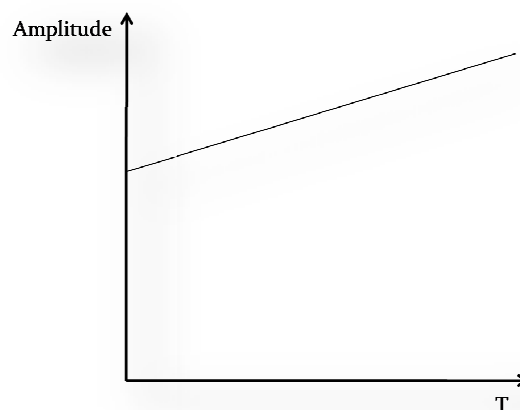


Fig 5.3: PI controller curve

5.3 Frequency converter:

Initially, the main reason for using frequency conversion technology is for speed control.

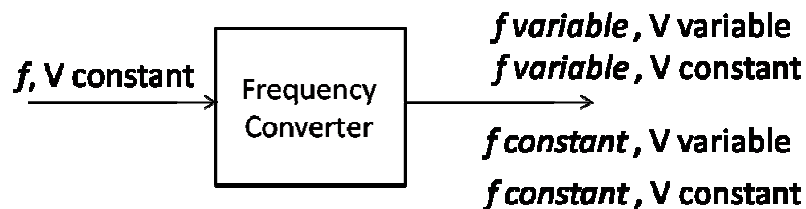


Fig 5.4: Frequency converter block diagram

The single phase frequency converter is applied already in application areas, as washing machines, air condition, and used for industrial application. It is used in motor control to control both control the frequency and voltage.

5.3.1 Frequency Converter Principles:

The normal household power supply or industrial power supply voltage and frequency is well defined and not open to change. The device, which takes this fixed voltage and frequency AC power and converts it into a variable voltage or variable frequency AC supply, is known as a Frequency Converter. In order to generate a variable voltage and frequency, the system must first rectify the AC input power source into DC after which the DC will be reconverted back into AC using the converter. The device, which converts the DC back into AC, and which can be controlled in both voltage and frequency, is known as the frequency converter. The frequency converter's output is a simulated sine wave whose main purpose is to control the speed of a synchronous motor. [7]

5.3.2 Variable Frequency:

As shown in Fig 5.5, that shows the relation between the frequency and voltage, from the f_1 to f_n the value of V/f is constant (k), in this case the value of torque remains constant, and when the voltage remains constant until reach the max frequency, in this case the power is remains constant. [7]

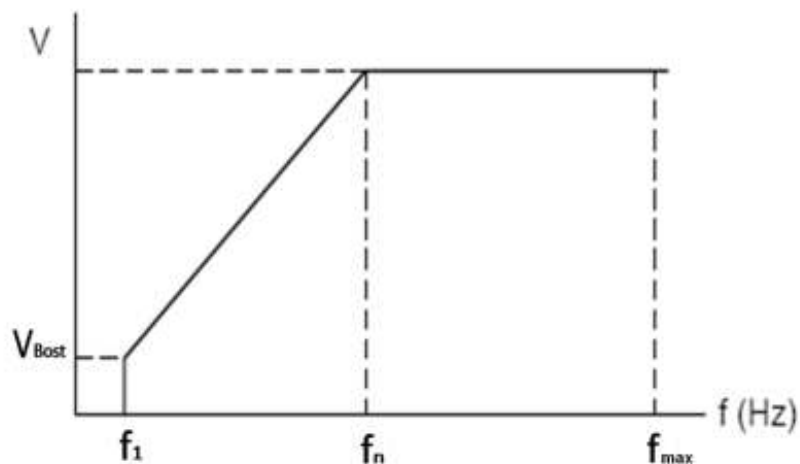


Fig 5.5: Relation between the voltage and frequency

The frequency of the voltage applied to the motor is smoothly changed from the value close to zero to the rated value. The motor runs synchronously during the entire starting period. Variable voltage variable frequency (VVVF) solid state inverters are commonly used.

As frequency variable the speed is variable, according to Equation (2.1)

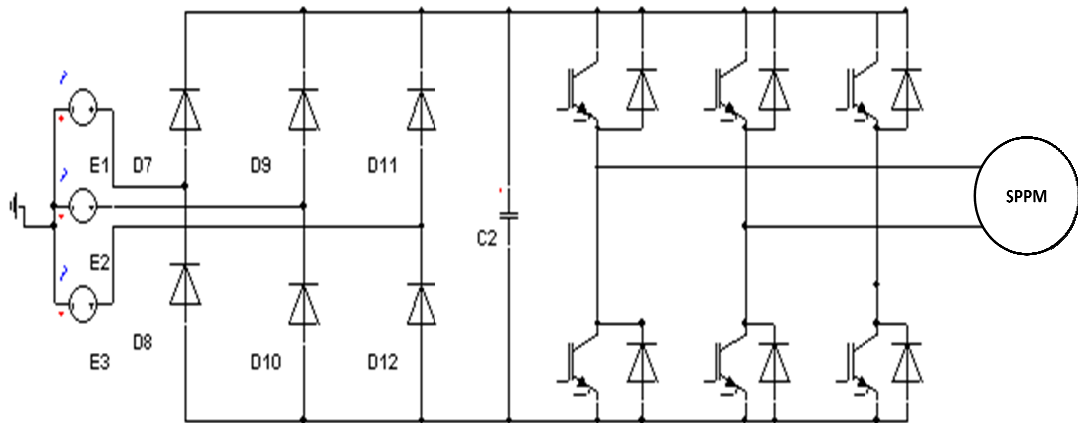


Fig 5.6: Three phase frequency converter construction using Simplorer

Using three phase frequency converter and taking the voltage gain from the frequency converter is about 70%, from the source voltage that is equal 380 V, to get voltage approximately equal 250V that is approximately the single phase voltage and then applying to motor.

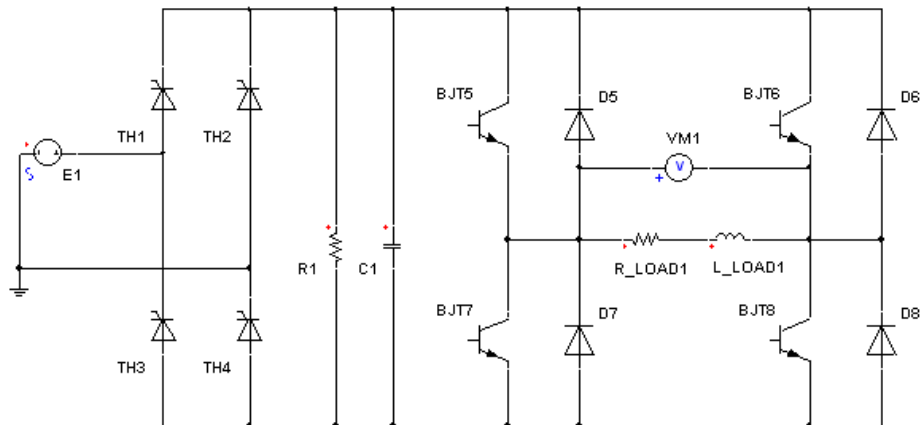


Fig 5.7: Single phase frequency converter construction using Simplorer

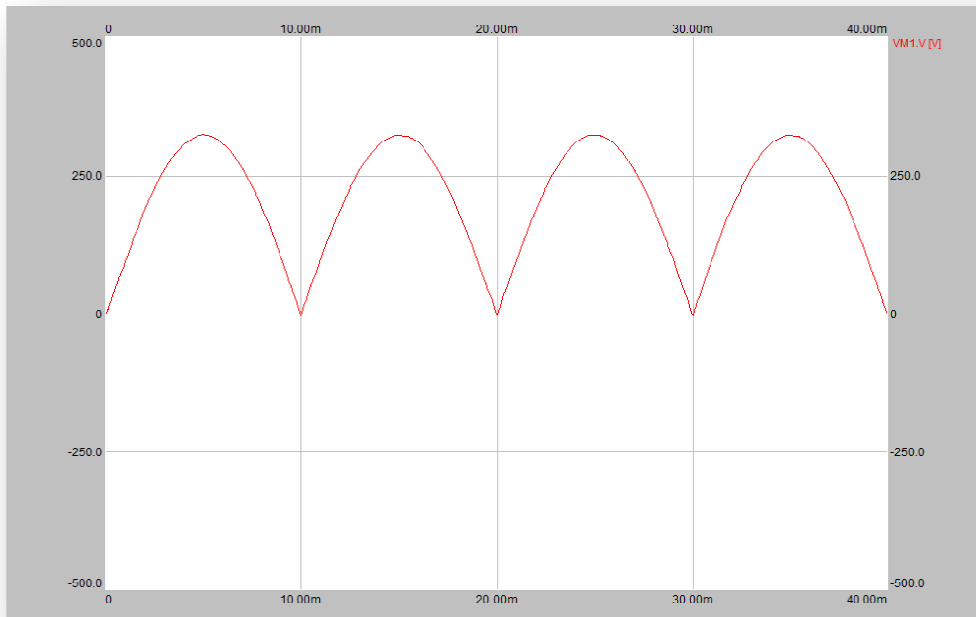


Fig 5.8: Output voltage from rectifier

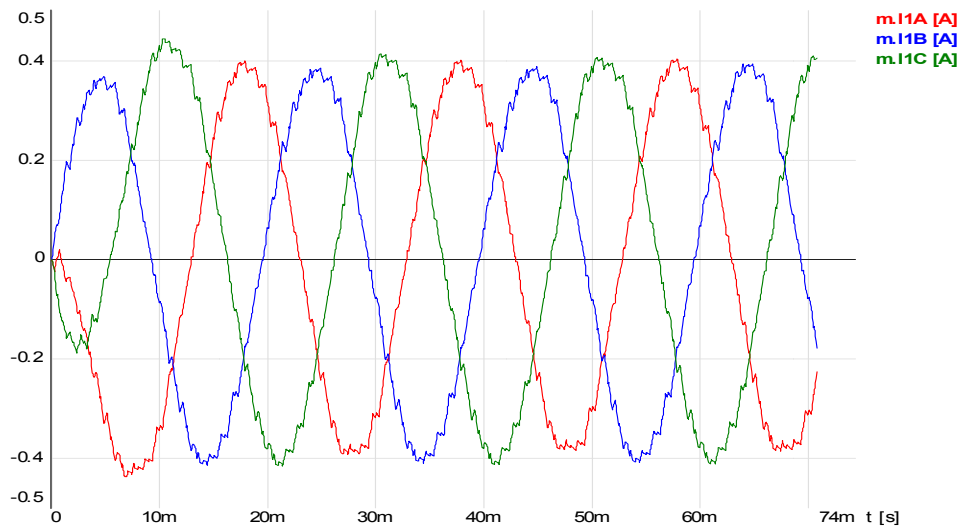


Fig 5.9: Output voltage from frequency converter

Conclusion:

In this project, the method of a designing of Single Phase Permanent Magnet (SPPM) motor is presented, in terms of motor dimensions and material properties, which are utilized in the dynamic model of the motor. The intention of the project is to develop means of SPPM performance calculations.

This motor has a special design of stator and rotor with non-uniform air-gaps, with U-shape design.

The behavior of the motor as (starting, torque...) is described, and also the starting behavior is described when the value of frequency reach eigenfrequency then the motor starts to move continuously.

The network method (equivalent circuit) is used to analyze magnetic circuit. It is usually used in the design of electric machines and transformers, and to perform the analytical solution of this project.

A frequency converter is used as control device to obtain suitable type of control for this motor.

There are growing applications of this motor, especially in low-power like automobile industry, central heating and house appliances (washing machines, dishwasher).

References:

- [1] Jacek F. Gieras, Mitchell Wing, **Permanent Magnet Motor Technology: Design and Applications**. 2nd edition, CRC Press, 2002.
- [2] Stephen J. Champman, **Electric Machinery Fundamentals**, 3rd edition, British Aerospace Australia.
- [3] Enrique L. Carrillo Arroyo, **Modeling and Simulation of Permanent Magnet Synchronous Motor Drive System**, University of Puerto Rico, 2006.
- [4] http://www.allaboutcircuits.com/vol_2/chpt_13/2.html.
- [5] Richard Torrens, **Permanent Magnet Motors**, 4QD, Aug. 2006, <http://www.4qd.co.uk/fea/pmm.html>.
- [6] Nise, Norman S., **Control Systems Engineering**, 4th Edition, John Wiley & Sons, October 2003.
- [7] Gopal K. Dubey, **Fundamentals of Electrical Drives**, Narosa Publishing house, 1995.
- [8] Richard L. Burden, J. Douglas Faires, **Numerical Analysis**, 7th Edition, Wadsworth Group, USA, 2001.

APPENDICES

APPENDIX A

Permanent Magnet Material

A.1 Permanent Magnet Material

PM are applied on a great scale in small electrical mechanical devices. A small amount of high qualified PM-material can cause a relative high magnetic field.

The PM is used for different kind of actuators like brushless motors, step-motors, linear motors and servo motors. Because no windings are necessary for developing a magnetic field is the efficiency higher than other motors. The thermal problems are better controllable. Permanent magnets make the construction lighter and compacter. [5]

PM's are also called hard magnetic materials, which mean ferromagnetic materials with a wide hysteresis loop. [5]

A (PM's) can produce magnetic flux in an air gap with no exciting winding and no dissipation of electric power. As any other ferromagnetic material, a PM can be described by its B-H hysteresis loop.

The NdFeB is also susceptible to corrosion. NdFeB magnets have great potential for considerably improving the performance-to-cost ratio for many applications. For this reason they have a major impact on the development and application of PM apparatus. [1]

There are two different types of rare-earth NdFeB PMs are classified into sintered PMs and bonded PMs. [1]

Table A.1 : Magnetic characteristics of sintered NdFeB PMs manufactured in China

Grade	Remanent magnetic flux density B_r , T	Coercivity H_c , kA/m	Intrinsic coercive force iH_c , kA/m	Maximum energy product $(BH)_{max}$, kJ/m ³
N27	1.02...1.10	764...836	≥ 955	199...223
N30	1.08...1.15	796...860	≥ 955	223...247
N33	1.13...1.17	844...884	≥ 955	247...263
N35	1.17...1.21	876...915	≥ 955	263...286
N38	1.20...1.28	899...971	≥ 955	286...302
N27M	1.02...1.10	764...836	≥ 1194	199...223
N30M	1.08...1.15	796...860	≥ 1194	223...247
N33M	1.13...1.17	844...884	≥ 1194	247...263
N35M	1.17...1.21	876...915	≥ 1194	263...286
N27H	1.02...1.10	764...836	≥ 1353	199...223
N30H	1.08...1.15	796...860	≥ 1353	223...247
N33H	1.13...1.17	844...884	≥ 1353	247...263
N35H	1.17...1.21	876...915	≥ 1353	263...286
N27SH	1.02...1.10	764...836	≥ 1592	199...223
N30SH	1.08...1.15	796...860	≥ 1592	223...247
N33SH	1.13...1.17	844...884	≥ 1592	247...263
N35SH	1.16...1.22	876...915	≥ 1592	263...279
N25UH	0.97...1.05	748...812	≥ 1910	183...207
N27UH	1.02...1.10	764...836	≥ 1910	199...223

Table A.2: Physical properties of sintered NdFeB PMs manufactured in China

Grade	Operating temperature °C	Curie temp °C	Specific mass density g/cm ³	Recoil permeability
N27	≤80	310	7.4...7.5	1.1
N30	≤80	310	7.4...7.5	1.1
N33	≤80	310	7.4...7.5	1.1
N35	≤80	310	7.4...7.5	1.1
N38	≤80	310	7.4...7.5	1.1
N27M	≤100	320	7.4...7.5	1.1
N30M	≤100	320	7.4...7.5	1.1
N33M	≤100	320	7.4...7.5	1.1
N35M	≤100	320	7.4...7.5	1.1
N27H	≤120	340	7.4...7.5	1.1
N30H	≤120	340	7.4...7.5	1.1
N33H	≤120	340	7.4...7.5	1.1
N35H	≤120	340	7.4...7.5	1.1
N27SH	≤150	340	7.4...7.5	1.1
N30SH	≤150	340	7.4...7.5	1.1
N33SH	≤150	340	7.4...7.5	1.1
N35SH	≤150	340	7.4...7.5	1.1
N25UH	≤170	340	7.4...7.5	1.1
N27UH	≤170	340	7.4...7.5	1.1

Table A.3: Magnetic characteristics of bonded NdFeB PMs manufactured in China.

Grade	Remanent magnetic flux density Br, T	Coercivity H _c , kA/m	Intrinsic coercive force iH _c kA/m	Maximum energy product (BH) _{max} , kJ/m ³
N36G	≥ 0.70	≥ 170	≥ 210	32...40
N44Z	≥ 0.47	≥ 360	≥ 540	40...48
N52Z	≥ 0.55	≥ 360	≥ 500	48...56
N60Z	≥ 0.58	≥ 380	≥ 680	56...64
N68G	≥ 0.60	≥ 410	≥ 1120	64...72
N76Z	≥ 0.65	≥ 400	≥ 720	70...80
N84Z	≥ 0.70	≥ 450	≥ 850	80...88

Table A.4: Physical properties of bonded NdFeB PMs manufactured in China.

Grade	Maximum operation temperature $^{\circ}\text{C}$	Temperature coefficient for Br $\%/^{\circ}\text{C}$	Curie temp. $^{\circ}\text{C}$	Specific mass density g/cm^3
N36G	70	≤ -0.13	300	6.0
N44Z	110	≤ -0.13	350	6.0
N52Z	120	≤ -0.13	350	6.0
N60Z	120	≤ -0.13	350	6.0
N68G	150	≤ -0.13	305	6.0
N76Z	150	≤ -0.13	360	6.0
N84Z	150	≤ -0.13	360	6.0

APPENDIX B

Motor Parameter Calculation

B.1 Motor Parameter Calculation

Table B.1: Motor parameters

Symbol	Value
A_m	$7.088 \cdot 10^{-2}$ mm
l_m	4.426 mm
μ_p	1.2947 mm Tesla/A
Λ_r	$2.073 \cdot 10^{-5}$ $\Omega \cdot m$
H_c	950 A/m
F_r	4.2047 A
Λ_{g1}	$8.95 \cdot 10^{-6}$ $\Omega \cdot m$
$\Lambda_g(\theta)$	$4.15 \cdot 10^{-6}$ $\Omega \cdot m$
\mathfrak{F}_r	4.205 A
x	1.7229 mm
$\Lambda_r(\theta_s)$	$1.9725 \cdot 10^{-5}$ $\Omega \cdot m$
z_g	25 mm
g_{r1}	12.71 mm
g_{r2}	33.3 mm
g_{r3}	2.8432 mm
g_r	16.2844 mm
θ_1	$74.357^\circ = 1.2978$ rad
θ_2	$17.04^\circ = 0.297$ rad
r_g	5.875 mm
$\Lambda_g(\theta_s)$	$7.12 \cdot 10^{-8}$ $\Omega \cdot m$
r_{g1}	5.75 mm
r_{g2}	6 mm
Torque	2.57 Ncm
θ_f	$34.47^\circ = 0.6016$ rad
g_f	11.44 mm
θ_{fe}	$20.24^\circ = 0.353$ rad
$\Lambda_{g1}(\theta_s)$	$5.675 \cdot 10^{-7}$ $\Omega \cdot m$
$\Lambda_{g2}(\theta_s)$	$4.737 \cdot 10^{-7}$ $\Omega \cdot m$
l_{r1}	4.246 mm
\mathfrak{F}_{s1}	4.0337 A
Λ_{g1} "for unit axial length of rotor"	$9.032 \cdot 10^{-8}$ $\Omega \cdot m$
ϕ_{g1}	$1.8059 \cdot 10^{-5}$ wb

ϕ_{g2}	$8.4128 \cdot 10^{-6}$ wb
ϕ_g	$2.64718 \cdot 10^{-5}$ wb
θ_0	$6.0399^\circ = 0.1054$ rad
R_1	13.5 mm
R_2	14.5 mm
θ_{S1}	$61^\circ = 1.06465$ rad
θ_{S2}	$50^\circ = 0.87266$ rad
R_s	13.95 mm
θ_s	$21.267^\circ = 0.37$ rad
y_r	13.63 mm
x_g	18.9 mm
x_r	11.54 mm
x'_g	18.366 mm
w_s	50 mm
w_f	70.2 mm
σ_s	0.83
σ_f	0.88
z_{sf}	33.5 mm
x_{sf}	8.424 mm
Λ_s	$1.246 \cdot 10^{-6}$ $\Omega \cdot m$
Number of turns (N)	1382 turns
Rotor diameter	9.5 mm
z_s	25 mm
g_1	2 mm
g_2	2.5 mm
$x_{wt} x_g$	54 mm
y_g	13 mm

To find the value of θ_0 by using Taylor Theorem: [8]

$$P_n(x) = f(x_0) + f'(x_0)(x - x_0) + \frac{f''(x_0)}{2!}(x - x_0)^2 + \dots + \frac{f^{(n)}(x_0)}{n!}(x - x_0)^n$$

$$\theta_0 = 6.0399^\circ$$